

Parallel, but Dissociable, Processing in Discrete Corticostriatal Inputs Encodes Skill Learning

Highlights

- Associative and sensorimotor inputs are co-engaged during early action learning
- Inputs disengage in a dissociable manner as actions are refined into skills
- Associative input disengagement predicts subsequent skill learning
- Somatic and presynaptic engagement diverges early in action learning

Authors

David A. Kupferschmidt,
Konrad Juczewski, Guohong Cui,
Kari A. Johnson, David M. Lovinger

Correspondence

lovindav@mail.nih.gov

In Brief

Kupferschmidt et al. probe real-time activity dynamics of associative and sensorimotor cortical projections to striatum during skill learning. They reveal substantive co-engagement and dissociable disengagement of the two pathways across learning and find that associative pathway disengagement predicts subsequent skill learning.

Parallel, but Dissociable, Processing in Discrete Corticostriatal Inputs Encodes Skill Learning

David A. Kupferschmidt,^{1,2} Konrad Juczewski,¹ Guohong Cui,³ Kari A. Johnson,¹ and David M. Lovinger^{1,4,*}

¹Section on Synaptic Pharmacology & In Vivo Neural Function, Laboratory for Integrative Neuroscience, National Institute on Alcohol Abuse and Alcoholism, US National Institutes of Health, Rockville, MD, USA

²Integrative Neuroscience Section, National Institute of Neurological Disorders and Stroke, US National Institutes of Health, Bethesda, MD, USA

³In Vivo Neurobiology Group, Neurobiology Laboratory, National Institute of Environmental Health Sciences, US National Institutes of Health, Research Triangle Park, NC, USA

⁴Lead Contact

*Correspondence: lovindav@mail.nih.gov

<https://doi.org/10.1016/j.neuron.2017.09.040>

SUMMARY

Changes in cortical and striatal function underlie the transition from novel actions to refined motor skills. How discrete, anatomically defined corticostriatal projections function *in vivo* to encode skill learning remains unclear. Using novel fiber photometry approaches to assess real-time activity of associative inputs from medial prefrontal cortex to dorsomedial striatum and sensorimotor inputs from motor cortex to dorsolateral striatum, we show that associative and sensorimotor inputs co-engage early in action learning and disengage in a dissociable manner as actions are refined. Disengagement of associative, but not sensorimotor, inputs predicts individual differences in subsequent skill learning. Divergent somatic and presynaptic engagement in both projections during early action learning suggests potential learning-related *in vivo* modulation of presynaptic corticostriatal function. These findings reveal parallel processing within associative and sensorimotor circuits that challenges and refines existing views of corticostriatal function and expose neuronal projection- and compartment-specific activity dynamics that encode and predict action learning.

INTRODUCTION

Motor skill learning is essential for optimizing behavior (Hikosaka et al., 2013) and is impaired in individuals with action control disorders like Huntington's and Parkinson's diseases (Heindel et al., 1988; Stefanova et al., 2000; Wu et al., 2015). During skill learning, neural control of actions is believed to shift from associative corticostriatal circuits, composed of neuronal inputs from prefrontal cortices to the dorsomedial striatum (DMS), to sensorimotor corticostriatal circuits, composed of neuronal inputs

from sensorimotor cortices (e.g., M1) to the dorsolateral striatum (DLS; McGeorge and Faull, 1989; Haber and Gdowski, 2003; Miyachi et al., 1997, 2002; Graybiel, 2008; Yin et al., 2009; Doyon et al., 2009). Prominent models of skill learning posit that a serial transfer of neural activity from associative to sensorimotor circuits underlies this shift in neural control (Miyachi et al., 2002; Lehéricy et al., 2005; Floyer-Lea and Matthews, 2005; Lohse et al., 2014). Indeed, several studies using functional magnetic resonance imaging (fMRI) or neuronal unit recordings from various nodes within rodent corticostriatal circuits report that associative brain regions are preferentially active and functionally connected during early action learning (Poldrack et al., 2005; Coynel et al., 2010; Yin et al., 2009), whereas sensorimotor brain regions are preferentially active and functionally connected when actions are refined into skills (Miyachi et al., 2002; Yin et al., 2009; Jueptner et al., 1997a, 1997b; Lehéricy et al., 2005; Floyer-Lea and Matthews, 2005; Koralek et al., 2013). Alternative models propose that the two circuits are simultaneously engaged during learning, show concurrent learning-related neural plasticity, and dynamically compete for control of performance (Yin et al., 2009; Thorn et al., 2010; Thorn and Graybiel, 2014; Bassett et al., 2015). These discrepancies likely stem from a reliance by both models on measures of regional activity and statistical coherence that cannot resolve the activity dynamics of discrete, anatomically defined projections. Thus, tracking real-time, learning-related changes in the activity of associative and sensorimotor cortical inputs to striatal subregions will refine and help disambiguate the circuit basis of action learning.

Similarly lacking from neural models of skill learning is an account of complex modulation of presynaptic function. Glutamate release from corticostriatal terminals, known to drive activity in striatal medium-sized spiny projection neurons (Wilson, 1995), is potently modulated by various presynaptic signaling and plasticity processes (Calabresi et al., 1990; Lovinger, 1991; Atwood et al., 2014; Park et al., 2014). *Ex vivo* electrophysiology and gene deletion studies predict roles for inhibitory plasticity of corticostriatal terminals in skill learning (Yin et al., 2009; Kheirbek et al., 2009; Hawes et al., 2015). However, monitoring presynaptic function in discrete corticostriatal projections *in vivo* during

learning is required to test these predictions and advance a more anatomically and physiologically constrained view of how cortex communicates with striatum to encode action learning.

RESULTS

Fiber Photometry to Assess *In Vivo* Activity of Corticostriatal Inputs

We designed novel *in vivo* fiber photometry (Cui et al., 2013, 2014; Gunaydin et al., 2014) approaches to assess projection-specific presynaptic activity dynamics of corticostriatal inputs during skill learning. We injected adeno-associated viruses (AAVs) encoding a Cre recombinase-dependent form of the genetically encoded Ca²⁺ indicator GCaMP6s into either the medial prefrontal cortex (mPFC) or the M1 of mice expressing Cre under the control of the Emx1 promoter (Emx1::Cre mice). GCaMP6s was thus expressed in mPFC or M1 pyramidal neurons and their dorsal striatal inputs, which preferentially innervate the DMS or DLS, respectively (Figures 1A and 1B). An optical fiber was implanted into the DMS or DLS to simultaneously deliver blue excitation light and collect GCaMP6s fluorescence from associative (mPFC-DMS) or sensorimotor (M1-DLS) inputs (Figure S1). Fluorescence was directed into a polychromator and 16-channel photomultiplier array coupled to a time-correlated single-photon counting (TCSPC) module to quantify bulk fluorescence across a range of wavelengths (Cui et al., 2013, 2014; Figures 1C and 1D). Experiments using photometric recordings of ex vivo fluorescent brain tissue determined that fluorescence detected by our fiber photometry system derives from a brain volume of ~0.02 mm³ (~450 μm from tip of fiber, ~375 μm at base of detection cone) that enables selective sampling from discrete striatal and cortical brain areas (Figures 1E–1I).

In freely moving mice showing GCaMP6s expression in mPFC-DMS or M1-DLS corticostriatal inputs, we commonly observed sustained movement-related changes in fluorescence intensity (Figure 2A). Changes were more prominent in spectral channels comprising the peak of the GCaMP6s spectra than in off-peak channels and were absent in mice expressing enhanced green fluorescent protein (eGFP) or in wild-type mice. Thus, these fluorescence changes are unlikely to reflect motion-related artifacts. Supporting the activity dependence of these fluorescent changes, isoflurane anesthesia reversibly reduced basal GCaMP6s fluorescence and GCaMP6s fluorescent events in presynaptic corticostriatal inputs (Figure 2B; Figure S2A). Moreover, local pharmacological manipulation of mPFC or M1 activity by microinfusion of picrotoxin or lidocaine bidirectionally altered GCaMP6s fluorescence in mPFC-DMS or M1-DLS inputs of freely moving mice (Figures 2C–2F; Figures S2D–S2J). Together, these data and our previously reported brain slice photometry findings (Kupferschmidt and Lovinger, 2015) indicate that changes in GCaMP6s fluorescence from presynaptic corticostriatal elements represent Ca²⁺ dynamics that serve as a proxy for *in vivo* presynaptic activity.

Corticostriatal Inputs Are Engaged during a Motor Task

To examine the relationship between corticostriatal input activity and motor actions, we measured GCaMP6s fluorescence in mPFC-DMS and M1-DLS inputs while mice performed on the

accelerating rotarod. GCaMP6s fluorescence increased in both inputs when mice were placed on the rotating rod, generally intensified as the rod accelerated from 4 to 40 revolutions per minute (rpm), causing mice to make progressively faster stepping movements, and returned to baseline after mice fell off the rod (Figures 2G–2J; Figures S2B and S2C). This increase in fluorescence was selective for wavelengths within the GCaMP6s spectrum and absent in eGFP-expressing mice, indicating that rotarod performance is associated with increased activity of both mPFC-DMS and M1-DLS inputs. We will subsequently refer to this performance-related increase in activity as “engagement.”

To probe the activity-related properties of the presynaptic signals that we observed during performance, we conducted simultaneous *in vivo* photometry and extracellular field recordings from anesthetized mice (Figure 3; Figure S3). mPFC or M1 electrical stimulation evoked increases in GCaMP6s fluorescence in mPFC-DMS or M1-DLS inputs that responded dynamically (and comparably) to changes in stimulation intensity, frequency, and duration. Notably, sustained 5–10 Hz stimulation of mPFC or M1 evoked sustained fluorescence increases in mPFC-DMS or M1-DLS inputs that closely mimicked those seen during rotarod performance (Figures 2G, 2H, 3G, and 3H; Figures S3C and S3D).

Corticostriatal Inputs Show Parallel, but Dissociable, Engagement across Skill Learning

To assess how movement-related activity of corticostriatal inputs changed with skill learning, we trained mice expressing GCaMP6s or eGFP in mPFC-DMS or M1-DLS inputs on the rotarod for 10 trials/day for 5 days and simultaneously recorded changes in task-related fluorescence. This training paradigm produces a characteristic pattern of motor skill learning, as evidenced by rapid increases in latency to fall off the rotarod across trials on day 1 and slower, incremental increases in latency to fall across days 2 to 5 (Figures 4A and 4D; Costa et al., 2004; Yin et al., 2009). High-speed video analysis of foot position confirmed that increases in latency to fall are accompanied by increases in average foot height (i.e., learned ability to remain atop the rotating rod) and reductions in foot height variability, consistent with the acquisition of a refined motor skill (Figures S4A–S4D; Cao et al., 2015). Importantly, mice targeted for photometric recordings of GCaMP6s or eGFP in mPFC-DMS or M1-DLS inputs performed indistinguishably on the rotarod (Figures S4E–S4G), consistent with immunohistochemical and whole-cell electrophysiology experiments demonstrating that GCaMP6s expression induced no overt neuronal toxicity (Figure S5).

Photometric recordings of task-related GCaMP6s fluorescence during rotarod learning revealed that mPFC-DMS inputs were weakly engaged during initial trials on day 1 of training (“naïve” stage) but rapidly increased and peaked in their task-related engagement by the final trials of day 1 (“early” stage; Figures 4B, 4C, and 4K). Interestingly, the magnitude of task-related fluorescence in these inputs rapidly decreased on day 2 of training, indicating “disengagement” of these afferents. This decrease persisted into the final trials of day 5 (“late” stage; Figures 4B, 4C, and 4K). M1-DLS inputs, however, were strongly engaged during the naïve and early learning stages and

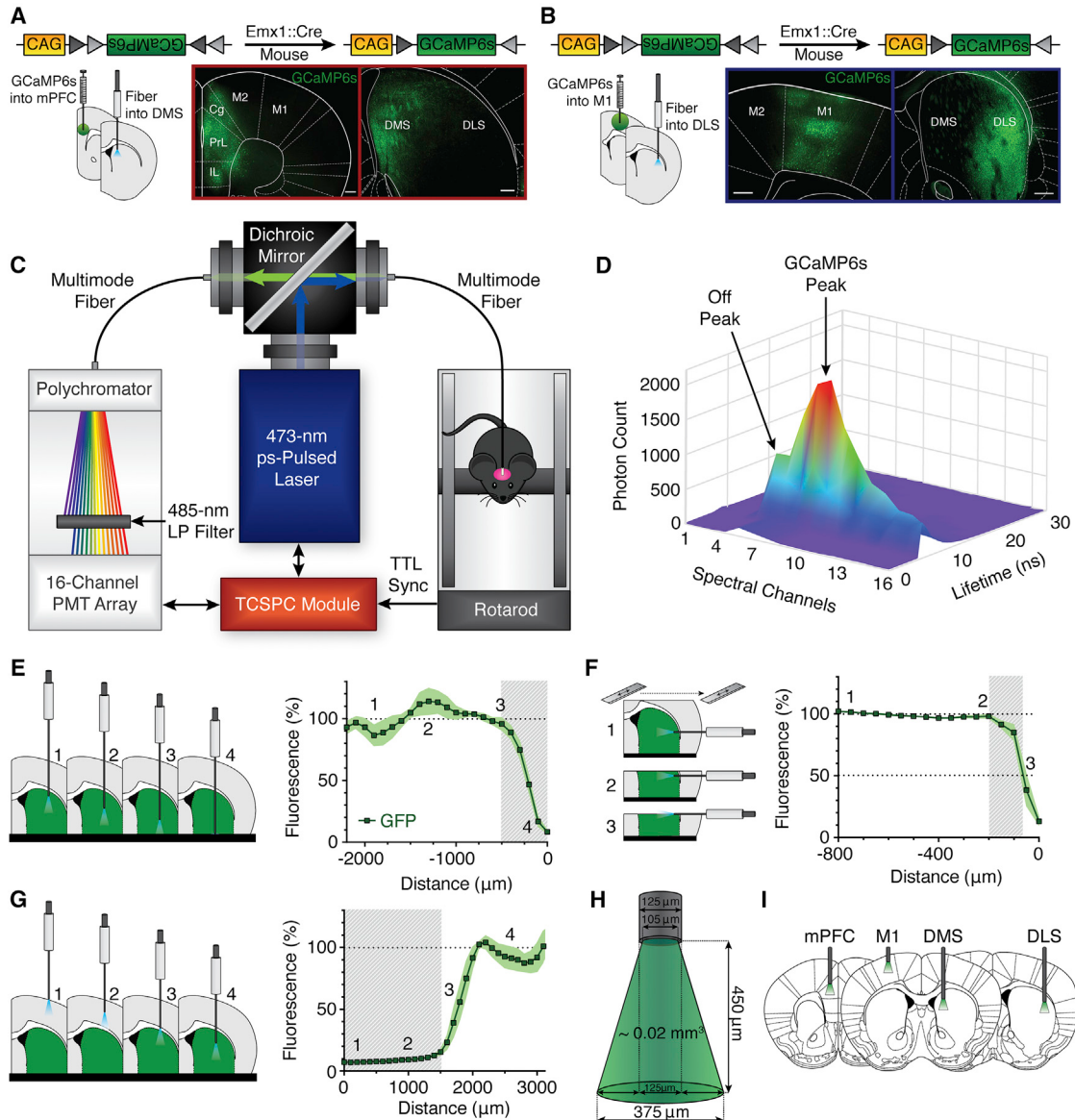


Figure 1. Fiber Photometry to Assess *In Vivo* Presynaptic Ca^{2+} Dynamics in Discrete Corticostriatal Inputs

(A) Diagram showing viral GCaMP6s injection into mPFC and optical fiber implantation into DMS of Emx1::Cre mice (top, left). GCaMP6s immunoreactivity in mPFC somata (middle) and DMS inputs (right).

(B) Diagram showing viral GCaMP6s injection into M1 and fiber implantation into DLS of Emx1::Cre mice (top, left). GCaMP6s immunoreactivity in M1 somata (middle) and DLS inputs (right). Scale bars, 200 μm .

(C) Diagram showing *in vivo* fiber photometry setup.

(D) 3D time-resolved spectrum obtained using TCSPC module from a mouse expressing GCaMP6s in sensorimotor inputs.

(E–G) Diagram (left) and results (right) of experiments using fluorescent brain tissue of mice expressing GFP in dopamine D2-receptor-expressing neurons ($n = 5$ D2R::GFP mice per experiment) designed to estimate the maximum depth of detection of the fiber photometry system (E), estimate the width of the detection cone of the photometry system (F), and assess any contribution of striatal fluorescence to signal detected from within cerebral cortex (G). See STAR Methods for full description. Fluorescence was derived from the same spectral channels used to detect peak GCaMP6s. Data in (E)–(G) are presented as mean \pm SEM.

(H and I) Diagram showing representative detection volume (H) in each of the four target brain sites (I; detection volume to scale with brain atlas).

See also Figure S1.

incrementally disengaged across training (Figures 4E, 4F, and 4K). Importantly, learning-related reductions in the magnitude of task-related fluorescence could not be attributed to bleaching

or loss of GCaMP6s expression over the training period (Figures 4G and 4H; Figures S4H and S6) and were indistinguishable in male and female mice (Figure 4I) and in left and right

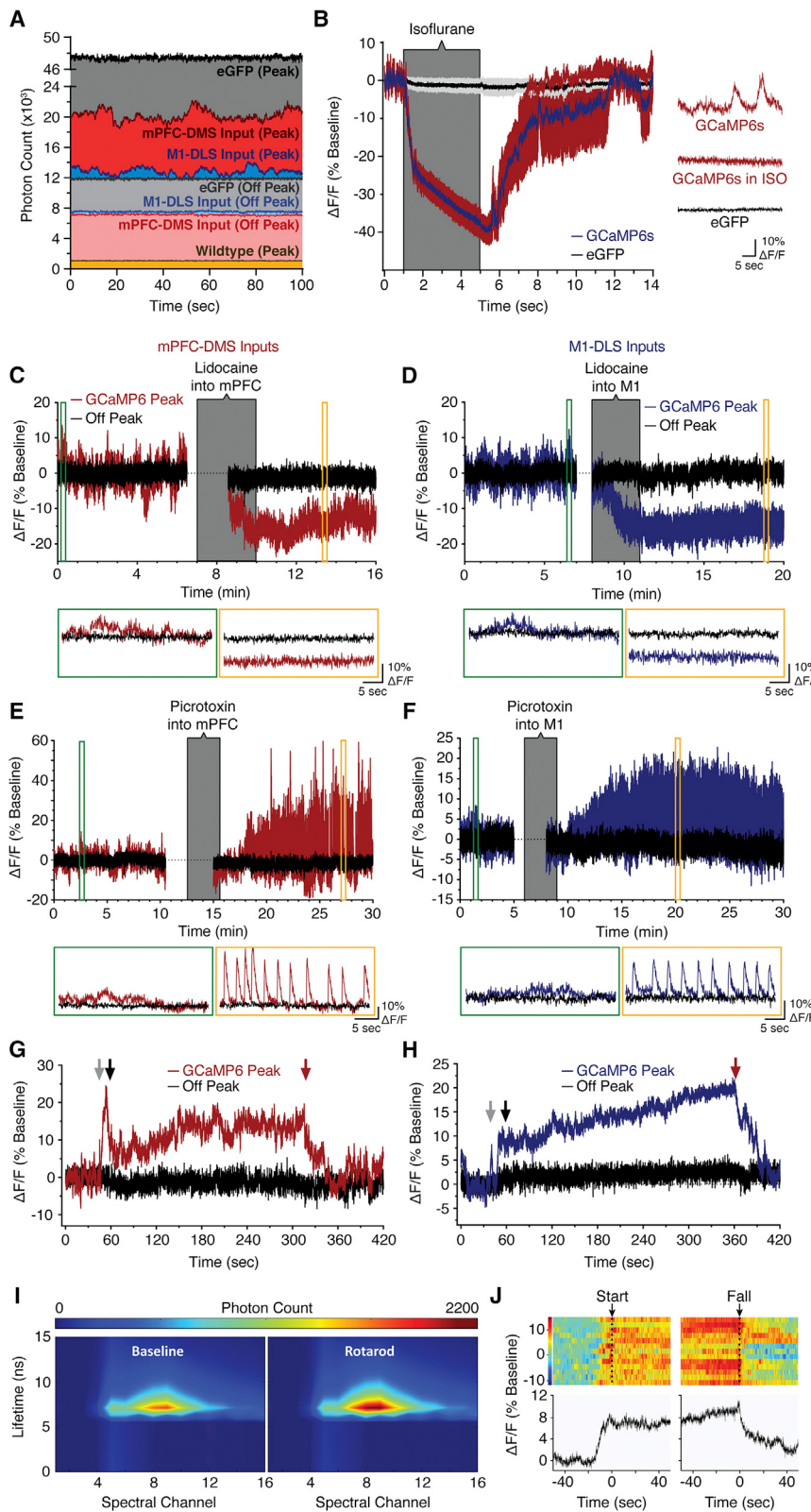


Figure 2. Discrete Cortical Inputs to the Striatum Are Engaged during Rotarod Performance

(A) Absolute fluorescence intensity recorded in DLS from freely moving mice with virally expressed GCaMP6s (mPFC-DMS, M1-DLS) or eGFP and wild-type mice.

(B) Isoflurane anesthesia (5% in oxygen, v/v) effects on basal fluorescence and fluorescent events in corticostriatal GCaMP6s- and eGFP-expressing mice ($n = 4/3$ GCaMP6s/eGFP). Data are presented as mean \pm SEM.

(C and D) Representative photometric recording of associative (C; mPFC-DMS) or sensorimotor (D; M1-DLS) inputs in response to infusion of lidocaine hydrochloride monohydrate (5%, 0.3 μ L) into mPFC (C) or M1 (D).

(E and F) Representative photometric recording of mPFC-DMS (E) or M1-DLS (F) inputs in response to local infusion of picrotoxin (0.25 μ g/ μ L, 0.3 μ L) into mPFC (E) or M1 (F). Periods of enhanced fluorescent events following mPFC infusion of picrotoxin were generally accompanied by periods of heightened locomotion, whereas individual fluorescent events following M1 infusion of picrotoxin were associated with myoclonic jerks in mouse forelimbs (predominantly contralateral to injection site).

(G and H) Representative rotarod trials from day 1 of training showing fluorescence changes in mPFC-DMS (G) and M1-DLS inputs (H). Gray, black, and red arrows denote retrieving mouse from rotarod base, trial start, and trial end, respectively.

(I) 2D color plot of absolute photon count and lifetime decay of GCaMP6s in M1-DLS inputs during baseline conditions and rotarod performance.

(J) Rotarod performance-related changes in sensorimotor input GCaMP6s fluorescence aligned to the start of the trial (left) or the end of the trial, when mice fell off of the rotarod (right; 13 trials from 4 mice).

See also Figure S2.

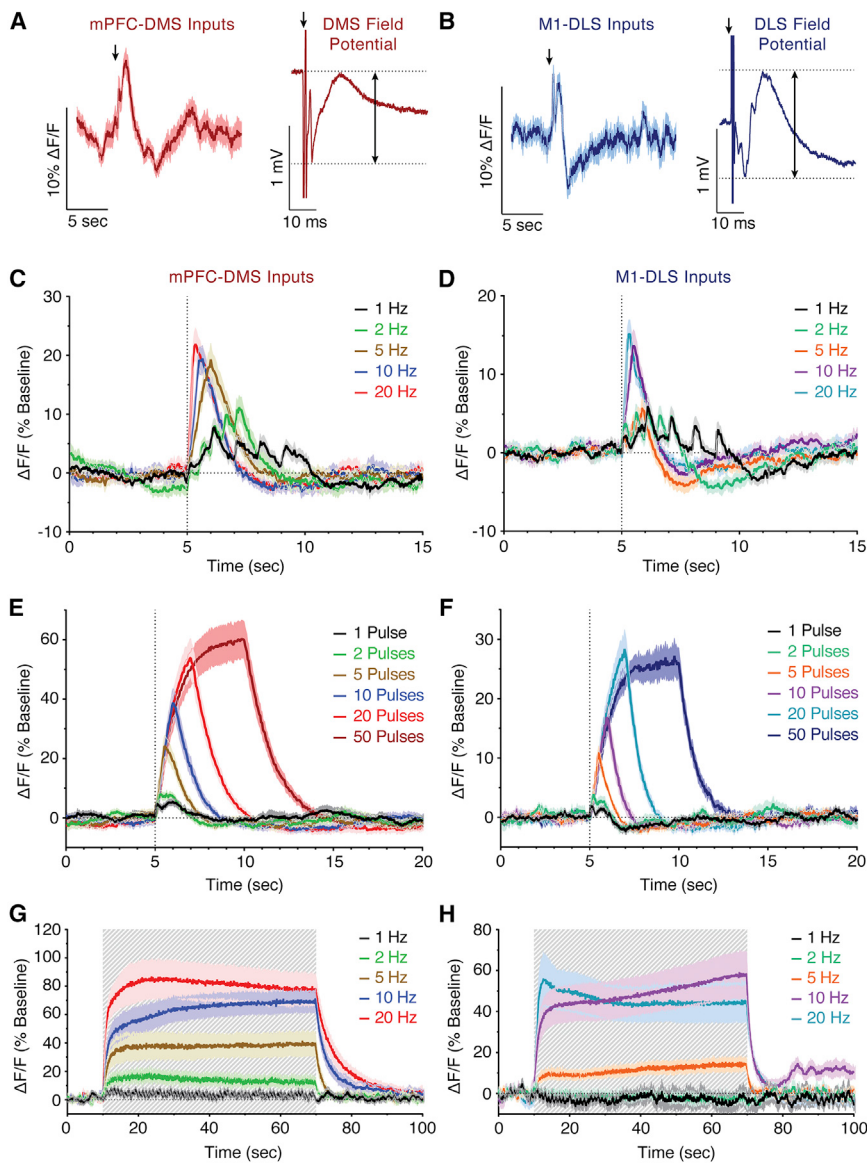


Figure 3. Simultaneous *In Vivo* Anesthetized Recordings of Electrically Evoked Pre-synaptic Ca^{2+} Transients in Corticostriatal Inputs and Striatal Field Potentials

(A and B) Photometric signals (left) and striatal field potentials (eFPs; right) recorded in DMS (A) or DLS (B) evoked by stimulation of mPFC (A) or M1 (B). Photometric, traces represent average of 40–53 stimulation trials; eFPs, traces represent single eFPs. Black arrows denote electrical stimulation.

(C and D) Photometric signals in mPFC-DMS (C) or M1-DLS inputs (D) in response to 5-pulse trains of stimulation in mPFC (C; $n = 6$ mice, 28 stimulation trials/frequency) or M1 (D; $n = 5$ mice, 17 stimulation trials/frequency) at varying frequencies.

(E and F) Photometric signals in mPFC-DMS (E) or M1-DLS inputs (F) in response to 10-Hz trains of electrical stimulation of mPFC (E; $n = 6$ mice, 28 stimulation trials/pulse number) or M1 (F; $n = 4$ –5 mice, 20–27 stimulation trials/pulse number) with varying pulse numbers.

(G and H) Photometric signals in mPFC-DMS (G) or M1-DLS inputs (H) evoked by 60-s electrical stimulation of mPFC (G; $n = 6$ mice, 8–11 stimulation trials/frequency) or M1 (H; $n = 6$ mice, 7–10 stimulation trials/frequency) at different frequencies.

Data in (C)–(H) are presented as mean \pm SEM; SEM was calculated using n of stimulation trials. See also Figure S3.

in the slopes of the mPFC-DMS and M1-DLS fluorescent signals during rotarod performance (Figures S7A–S7F). The fluorescence during task performance generally showed an upward slope that was strongest in the early stages of skill learning and showed reductions with training in both pathways (Figures S7A–S7C). mPFC-DMS input signals showed a modestly more rapid reduction in slope following early learning than M1-DLS input signals (Figure S7C). To assess whether the slopes of the signals of mPFC-DMS and M1-DLS inputs

hemispheres (Figure 4J). To directly compare activity profiles of these inputs, we normalized data from each mouse to its peak trial activity. Although differentially engaged at various stages of action learning, mPFC-DMS and M1-DLS inputs were substantively coactive, and both disengaged as actions were learned (Figure 4L). Together, these data provide direct evidence that associative and sensorimotor inputs show parallel (but dissociable) activity dynamics and concurrently engage their striatal targets at many stages of action learning (Thorn et al., 2010; Thorn and Graybiel, 2014; Bassett et al., 2015; Costa et al., 2004). Moreover, both inputs reduce their activity, albeit with different time courses and to different extents, as skilled actions are learned (Wu et al., 2004, 2008; Gobel et al., 2011; Mazzoni, 2008; Kawai et al., 2015).

To further probe the relationship between corticostriatal input activity and skill learning, we assessed learning-related changes

related to acceleration of the rotarod, we trained a subset of GCaMP6s-expressing mice previously trained for 5 days on the 4–40 rpm paradigm on “double acceleration” (8–80 rpm) and “no acceleration” (25 rpm) paradigms. Slopes of M1-DLS input signals were selectively enhanced when rotarod acceleration was increased to 8–80 rpm (Figures S7D–S7F). Notably, slopes of the fluorescent signals in mPFC-DMS and M1-DLS inputs induced by sustained electrical stimulation of cortex in anesthetized mice varied more by stimulation frequency (which controls frequency of afferent firing) than current intensity (which controls the extent of activated cortical tissue; Figures 3G and 3H; Figures S3C and S3D). This suggests that the upward slope observed during behavior depends on the frequency of afferent activation and changes in slope seen across skill learning or different acceleration paradigms may predominantly reflect changes in the patterning of activity in a population of striatal-projecting cortical

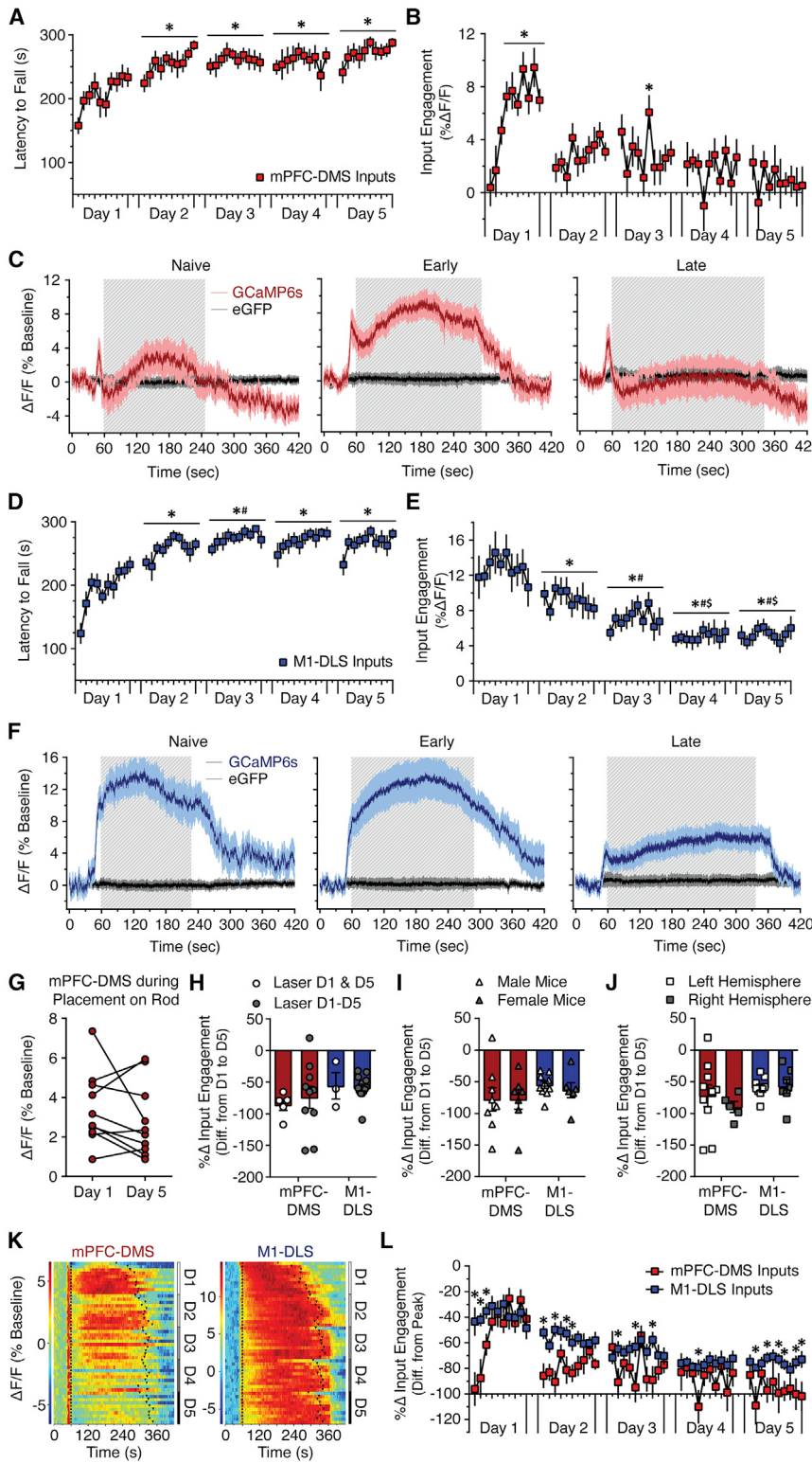


Figure 4. Associative and Sensorimotor Inputs Show Parallel, but Dissociable, Engagement across Skill Learning

(A) Rotarod performance in mice with GCaMP6s in mPFC-DMS inputs ($n = 11$; main effect of day, $F_{4,490} = 33.967$, $p < 0.001$, hierarchical linear mixed model [HLMM]; *different from day 1 [D1], $p < 0.001$).

(B) mPFC-DMS input engagement (percent baseline $\Delta F/F$ during rotarod performance) across trials (day \times trial interaction, $F_{36,483} = 2.74$, $p < 0.001$, HLMM; *different from day 1 trial 1 [D1T1], $p < 0.05$).

(C) Average trial-related fluorescent signals in mPFC-DMS inputs during naive (D1T1-3), early (D1T8-10), and late (D5T8-10) stages of training from GCaMP6s- and eGFP-expressing mice.

(D) Rotarod performance in mice with GCaMP6s in M1-DLS inputs ($n = 13$; main effect of day, $F_{4,586} = 92.66$, $p < 0.001$, HLMM; *different from D1, $p < 0.001$; #different from D2, $p < 0.05$).

(E) M1-DLS input engagement (percent baseline $\Delta F/F$ during rotarod performance) across trials (main effect of day, $F_{4,569} = 72.70$, $p < 0.001$, HLMM; *different from D1, $p < 0.001$; #different from D2, $p < 0.001$; \$different from D3, $p < 0.01$).

(F) Average trial-related fluorescent signals in M1-DLS inputs during naive, early, and late stages from GCaMP6s- and eGFP-expressing mice.

(G) mPFC-DMS input engagement during placement from base of the rotarod onto the rod was unchanged from days 1 and 5 of training ($n = 10$, $t_9 = 1.145$, $p = 0.282$, Student's paired t test).

(H) Changes in task-related fluorescence across days 1 to 5 in mPFC-DMS ($t_{13} = 0.4576$, $p = 0.655$, Student's unpaired t test) and M1-DLS input mice ($t_{14} = 0.202$, $p = 0.843$, Student's unpaired t test) that received blue laser illumination during training only on days 1 and 5 (laser on D1 and D5) or throughout training on all days (laser on D1–D5).

(I) Changes in task-related fluorescence across days 1 to 5 in female and male mPFC-DMS ($t_{13} = 0.0043$, $p = 0.997$, Student's unpaired t test) and M1-DLS ($t_{14} = 0.723$, $p = 0.482$, Student's unpaired t test) input mice.

(J) Changes in task-related fluorescence across days 1 to 5 in mPFC-DMS ($t_{13} = 0.696$, $p = 0.499$, Student's unpaired t test) and M1-DLS ($t_{14} = 0.163$, $p = 0.873$, Student's unpaired t test) input mice recorded from the left or right hemisphere.

(K) Rasterplots of percent baseline $\Delta F/F$ in mPFC-DMS (left) and M1-DLS (right) inputs across trials. (L) Trial-related engagement (percent baseline $\Delta F/F$) in mPFC-DMS and M1-DLS input mice normalized to their peak individual trial-related fluorescence (main effect of group, $F_{1,22} = 9.06$, $p < 0.01$, HLMM; group \times day \times trial interaction, $F_{45,1052} = 1.750$, $p < 0.005$, HLMM; *different from mPFC-DMS, $p < 0.05$).

Data in (A)–(F), (H)–(J), and (L) are presented as mean \pm SEM.

See also Figures S4–S6.

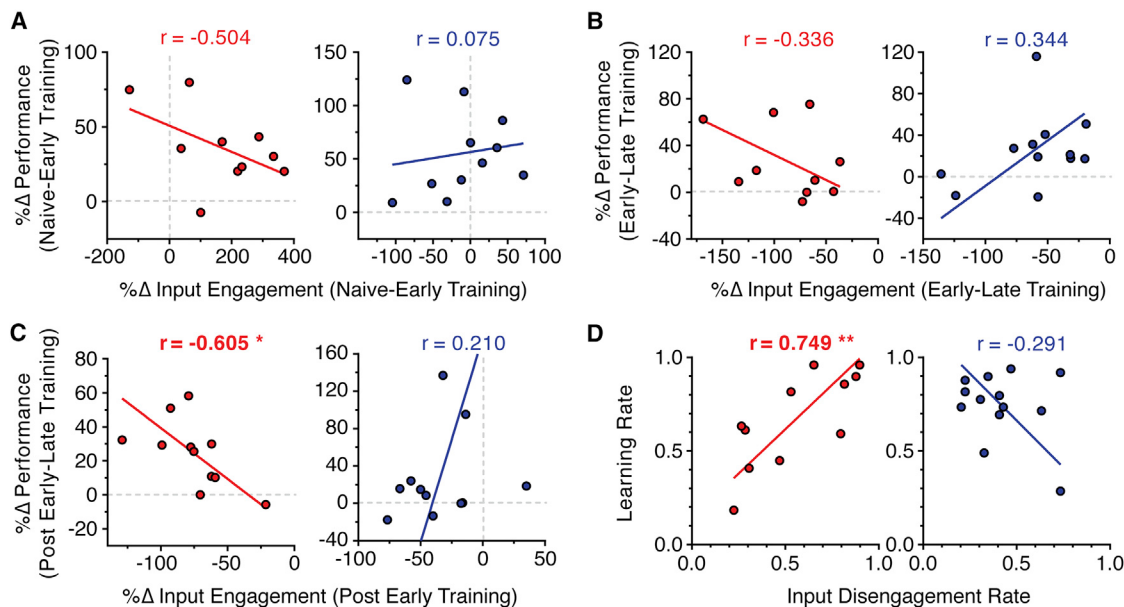


Figure 5. Disengagement of Associative Inputs Predicts Skill Learning

(A) Correlation between percent change in input engagement and percent change in latency to fall within day 1 of training (from day 1, trial 1-2 [D1T1-2] to day 1, trial 9-10 [D1T9-10]). mPFC-DMS (left, $r = -0.504$, $F_{1,8} = 2.722$, $p = 0.138$, Deming regression; Pearson, 1901); M1-DLS (right, $r = 0.075$, $F_{1,9} = 0.052$, $p = 0.826$, Deming regression).

(B) Correlation between percent change in input engagement and percent change in latency to fall from the end of day 1 (D1T9-10) to the end of day 5 of training (D5T9-10). mPFC-DMS (left, $r = -0.336$, $F_{1,8} = 1.020$, $p = 0.342$, Deming regression); M1-DLS (right, $r = 0.344$, $F_{1,10} = 1.340$, $p = 0.274$, Deming regression).

(C) Correlation between percent change in input engagement immediately following early training (from D1T9-10 to D2T1-2) and percent change in latency to fall during post-early-late training (from D2T1-2 to D5T9-10) to assess whether early changes in engagement were predictive of subsequent changes in performance. mPFC-DMS (left, $r = -0.605$, $F_{1,9} = 5.196$, * $p < 0.05$, Deming regression); M1-DLS (right, $r = 0.210$, $F_{1,9} = 0.415$, $p = 0.536$, Deming regression).

(D) Correlation between the input disengagement rate and the learning rate following peak input engagement (see STAR Methods). mPFC-DMS (left, $r = 0.749$, $F_{1,9} = 11.48$, ** $p < 0.01$, Deming regression); M1-DLS (right, $r = -0.291$, $F_{1,11} = 1.019$, $p = 0.335$, Deming regression).

neurons rather than changes in the proportion of task-activated corticostriatal neurons (see Costa et al., 2004).

Corticostriatal Input Dynamics Differentially Predict Skill Learning

We next assessed whether training-related changes in corticostriatal input activity correlated with skill learning. Input engagement within day 1 and disengagement across days 1 to 5 were uncorrelated with coincident improvements in performance (Figures 5A and 5B). However, the magnitude of disengagement of mPFC-DMS inputs immediately following early training was predictive of higher performance gains across subsequent training (Figure 5C). Moreover, the rate of disengagement of mPFC-DMS inputs positively correlated with the rate at which individual mice achieved their maximum performance (Figure 5D). These findings indicate that activity of mPFC inputs to the DMS may help to gate the transition from unskilled to skilled actions, perhaps by impeding access of sensorimotor circuits to the control of skilled performance (Yin et al., 2009; Thorn et al., 2010; Thorn and Graybiel, 2014; Bassett et al., 2015).

Establishing Feasibility to Monitor Real-Time Presynaptic Modulation during Skill Learning

Given that corticostriatal projections show forms of presynaptic modulation that have been implicated in skill learning (Yin et al.,

2009; Park et al., 2014; Kheirbek et al., 2009; Hawes et al., 2015), we next sought to assess whether the learning-related changes in the presynaptic activity we observed reflect broader circuit-level changes in the engagement of the corticostriatal projections or modulation at corticostriatal terminals specifically. To do so, we monitored upstream somatic activity of cortical neurons giving rise to associative and sensorimotor projections during skill learning. Differential changes in the average somatic and presynaptic activity of these projections could provide evidence of real-time presynaptic modulation during skill learning.

We first assessed our ability to measure task-related changes in GCaMP6s fluorescence in projection neurons in cortex. Specifically, we injected AAV1.CAG.FLEX.GCaMP6s virus into M1 of mice expressing Cre under the control of the Rbp4 promoter (Rbp4::Cre mice), resulting in GCaMP6s expression in a broad population of layer V M1 pyramidal neurons. We then implanted these mice with an optical fiber in M1 (Figure 6A). Photometric recordings from these mice provided a proxy for “somatic” activity (i.e., Ca^{2+} dynamics in local M1 somata, dendrites, and [presumably to a lesser degree] axon terminals). The signals recorded from “M1 Rbp4 somata” constituted slow, sustained fluorescence increases that closely resembled our presynaptic recordings, often with superimposed discrete fluorescent transients (Figure 6B; Figures S4I–S4K).

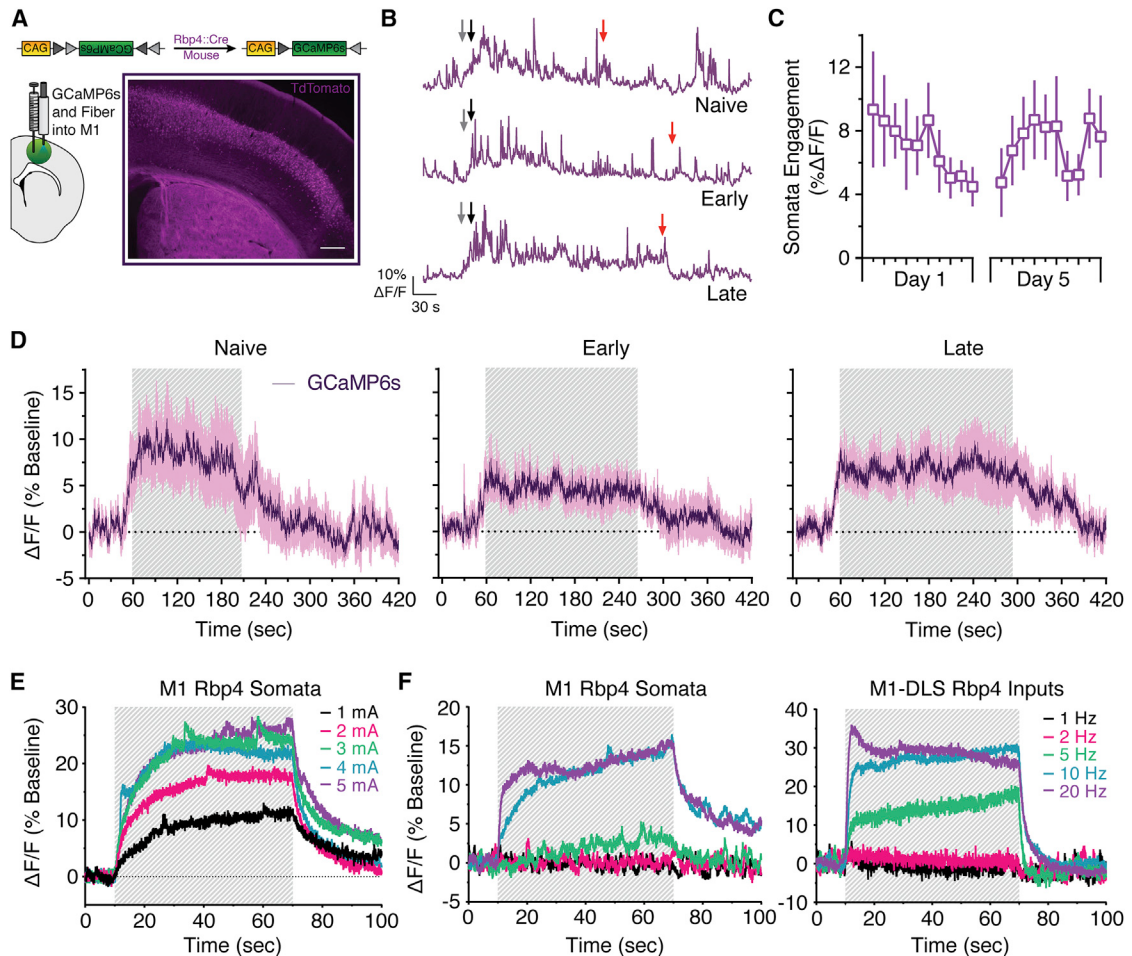


Figure 6. Photometric Recordings of M1 Rbp4::Cre-Expressing Layer V Pyramidal Neuron Somata during Skill Learning

(A) Diagram showing GCaMP6s injection and optical fiber implantation into M1 of Rbp4::Cre mice to target layer V somata (left). tdTomato expression in M1 of Rbp4::Cre;TdTomato mouse. Scale bar, 300 μ m.

(B) Representative rotarod trials showing fluorescence changes in M1 Rbp4 somata during naive, early, and late stages. Gray, black, and red arrows denote retrieving mouse from rotarod base, trial start, and trial end, respectively.

(C) M1 Rbp4 somata engagement (percent baseline $\Delta F/F$ during rotarod performance) across trials (main effect of day, $F_{1,95} = 0.077$, $p = 0.782$; main effect of trial, $F_{9,95} = 1.234$, $p = 0.284$, HLMM).

(D) Average trial-related fluorescent signals in M1 Rbp4 somata during naive, early, and late stages from GCaMP6s-expressing mice. Data in (C) and (D) are presented as mean \pm SEM.

(E and F) *In vivo* anesthetized recordings of electrically evoked GCaMP6s photometric signals in M1 somata and M1-DLS inputs from Rbp4::Cre mice. Photometric signals in M1 Rbp4 somata evoked by 60 s electrical stimulation of M1 (E; $n = 1$ mouse, 2 stimulation trials/intensity). Photometric signals in M1 Rbp4 somata (left) and DLS inputs from M1 Rbp4 somata (right) evoked by 60-s electrical stimulation of M1 (F; $n = 2$ –3 mice, 2–8 stimulation trials/frequency).

See also Figures S3 and S4.

Performance on the rotarod (Figure S4G) caused task-related increases in GCaMP6s fluorescence in M1 Rbp4 somata (Figures 6B–6D). As seen in M1-DLS inputs, M1 Rbp4 somata showed robust engagement during initial rotarod trials. In contrast, however, M1 Rbp4 somata showed no significant reduction of task-related activity after 5 days of training (Figures 6B–6D).

To assess the activity-related properties of the somatic fluorescence signal we observed during performance, and to probe whether somatic and presynaptic recordings yield comparable activity-related nonlinearities that warrant their direct compari-

son, we conducted *in vivo* photometry recordings from anesthetized mice expressing GCaMP6s in M1 Rbp4 neurons. As seen in M1-DLS inputs, M1 Rbp4 somata showed fluorescence changes that responded dynamically to changes in the intensity, frequency, and duration of local M1 electrical stimulation (Figures 6E and 6F; Figures S3E and S3G). Sustained 10–20 Hz stimulation of M1 evoked sustained fluorescence increases in M1 Rbp4 somata that closely mimicked those seen during rotarod performance (Figures 6D–6F; Figures S3I and S4I). Moreover, although smaller and more variable due to their higher propensity for spontaneous discrete fluorescent transients, M1 Rbp4 somatic

signals displayed activity-related nonlinearities that resembled those seen in presynaptic recordings of M1-DLS inputs from these same mice (Figure 6F; Figures S3F, S3H, and S3J) and GCaMP6s-expressing Emx1::Cre mice (Figures 3D, 3F, and 3H; Figure S3D). Together, these data demonstrate that photometric signals from cortical somata and striatal inputs respond proportionately to changes in activity, justifying our efforts to compare their task-related activities and test for any divergences across skill learning.

Monitoring for Real-Time Presynaptic Modulation during Skill Learning

Having established this proportionality, we next sought to assess learning-related changes in the somatic activity of DMS- and DLS-projecting mPFC and M1 neurons and compare these changes to those seen in mPFC-DMS and M1-DLS inputs. Despite the seeming elegance (i.e., within-subjects design) of expressing GCaMP6s in mPFC or M1 pyramidal neurons, implanting fibers into both the striatum and cortex of the same mouse, and recording from both sites simultaneously, this approach would unsatisfyingly compare a target-defined set of striatal inputs with a mixed population of target-undefined cortical pyramidal neurons.

Therefore, we used a dual-virus approach to selectively monitor the activity of cortical neurons that innervate a particular discrete striatal subregion. By injecting a Cre-encoding herpes simplex virus (HSV) that retrogradely transports from presynaptic terminals to somata (Gremel et al., 2016) into the DMS and a Cre-dependent GCaMP6s virus into the mPFC of wild-type mice, we selectively expressed GCaMP6s in DMS-projecting mPFC neurons that give rise to mPFC-DMS inputs (referred to as mPFC-DMS somata). Similarly, by coupling HSV-Cre virus in the DLS with Cre-dependent GCaMP6s virus in M1, we selectively expressed GCaMP6s in DLS-projecting M1 neurons that give rise to M1-DLS inputs (M1-DLS somata; Figures 7A and 7E; Figure S1). Optical fibers were implanted into the mPFC or M1 to assess activity of mPFC-DMS or M1-DLS somata during skill learning (Figures 7A and 7E; Figures S1, S4F, and S4G).

mPFC-DMS somata were slowly engaged across training on day 1 and rapidly disengaged from day 2 onward (Figures 7B–7D; Figure S7G). Activity of M1-DLS somata rapidly diminished across training on day 1 and remained low across subsequent training days (Figures 7F–7H; Figure S7H). Notably, the learning-related reduction in engagement of M1-DLS somata differed from the sustained engagement of the broader, target-undefined population of layer V pyramidal somata recorded in M1 of Rbp4::Cre mice (Figures 6C and 8A). This divergence could not be accounted for by between-group differences in rotarod performance (Figure S4G) or by obvious differences in the activity dependence of the fluorescent signals of the two cortical neuron populations, as they responded comparably to sustained electrical stimulation in anesthetized mice (Figures S3I–S3L). Therefore, this finding provides evidence that different populations of M1 neurons dissociated by their downstream target may differentially encode skill learning and suggests a preferential learning-induced disengagement of striatal-projecting M1 neurons (see Costa et al., 2004; Masmizu et al., 2014).

Largely consistent with learning-related patterns of mPFC-DMS and M1-DLS input activity, direct comparison of the somatic activity patterns of these pathways revealed that mPFC-DMS somata peaked in their engagement after initial action learning, whereas M1-DLS somata engagement peaked during initial performance (Figure 8B). However, to formally assess whether the activity of corticostriatal somata and presynaptic inputs changed differently with skill learning, we normalized data from each mouse to its peak trial somatic or presynaptic activity. Interestingly, mPFC-DMS somata were slower to reach peak engagement during early learning than were presynaptic mPFC-DMS inputs (Figure 8C). M1-DLS somata were more rapidly disengaged during early learning than presynaptic M1-DLS inputs (Figure 8D). Importantly, these differing time courses of somatic and presynaptic engagement could not be accounted for by differences in rotarod performance between any of the groups (Figure S4F). Therefore, these findings provide intriguing *in vivo* evidence consistent with local, real-time potentiation of presynaptic Ca^{2+} -related corticostriatal function during action learning (Figure 8E).

DISCUSSION

Here we probed the endogenous *in vivo* activity dynamics of discrete, anatomically defined corticostriatal projections in freely moving mice during skill learning. We showed that associative and sensorimotor inputs are concurrently active during the selection and shaping of novel actions and reduce their activity in a dissociable manner as actions are refined into skills. Disengagement of associative inputs selectively predicted individual differences in subsequent skill learning. We further showed neuronal compartment-specific activity that is consistent with a role for potentiated presynaptic corticostriatal function *in vivo* during action learning.

The parallel activity dynamics we observed in mPFC-DMS and M1-DLS inputs as mice refined their performance on the accelerating rotarod challenge models proposing a simple, serial transfer of activity from associative to sensorimotor circuits across skill learning (Miyachi et al., 2002; Lohse et al., 2014; Le-héricy et al., 2005; Floyer-Lea and Matthews, 2005). Indeed, by probing previously inaccessible aspects of corticostriatal activity, we revealed that key projections within the two circuits are concurrently engaged at many stages of learning to shape striatal plasticity and output (Figure 8E). Our finding that mPFC-DMS inputs and somata are preferentially engaged in early stages of skill learning advances the view that cognitive and attentional control networks help to encode early action learning but diminish their involvement as actions become well learned (Kelly and Garavan, 2005; Lohse et al., 2014; Bassett et al., 2015; Wu et al., 2004, 2008). Moreover, this transient engagement of mPFC-DMS projection neurons may underlie the preferential engagement of the associative striatum (DMS/caudate) seen during early skill learning across species using fMRI and neuronal unit recordings (Miyachi et al., 2002; Yin et al., 2009; Kelly and Garavan, 2005; Lohse et al., 2014). However, the pattern of strong initial engagement and subsequent disengagement of M1-DLS projections runs counter to reports of heightened task-related activity in the sensorimotor striatum

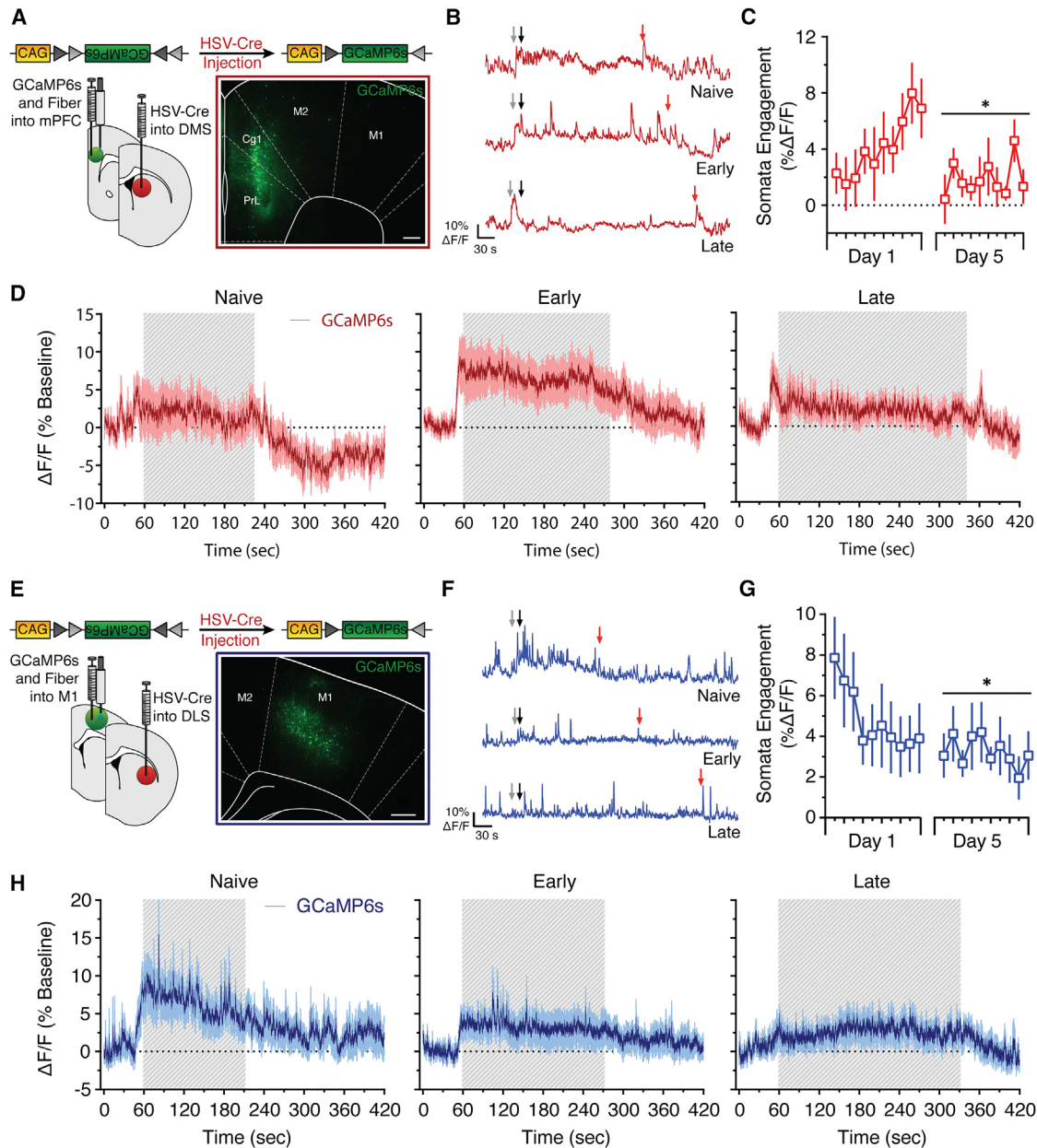


Figure 7. Associative and Sensorimotor Somata Are Differentially Engaged across Skill Learning

(A) Diagram showing HSV-Cre injection into DMS and GCaMP6s injection and optical fiber implantation into mPFC of C57BL/6J mice (top, left). GCaMP6s immunoreactivity in DMS-projecting mPFC somata (mPFC-DMS somata). Scale bars, 200 μ m.

(B) Representative fluorescence changes in mPFC-DMS somata from rotarod trials during naive, early, and late stages. Gray, black, and red arrows denote retrieving mouse from rotarod base, trial start, and trial end, respectively.

(C) mPFC-DMS somata engagement (percent baseline $\Delta F/F$ during rotarod performance) across trials ($n = 10$ mice; main effect of day, $F_{1,169} = 14.047$, $p < 0.001$, HLMM; *different from D1, $p < 0.001$).

(D) Average trial-related GCaMP6s signals of mPFC-DMS somata during naive, early, and late stages.

(E) Diagram showing HSV-Cre injection into DLS and GCaMP6s injection and fiber implantation into M1 of C57BL/6J mice (top, left). GCaMP6s immunoreactivity in DLS-projecting M1 somata (M1-DLS somata). Scale bar, 200 μ m.

(F) Representative fluorescence changes in M1-DLS somata from rotarod trials during naive, early, and late stages.

(G) M1-DLS somata engagement (percent baseline $\Delta F/F$ during rotarod performance) across trials ($n = 7$ mice; main effect of day, $F_{1,112} = 15.087$, $p < 0.001$, HLMM; *different from D1, $p < 0.001$).

(H) Average trial-related GCaMP6s signals of M1-DLS somata recorded during naive, early, and late stages.

Data in (C), (D), (G), and (H) are presented as mean \pm SEM.

See also Figures S1, S3, S4, and S7.

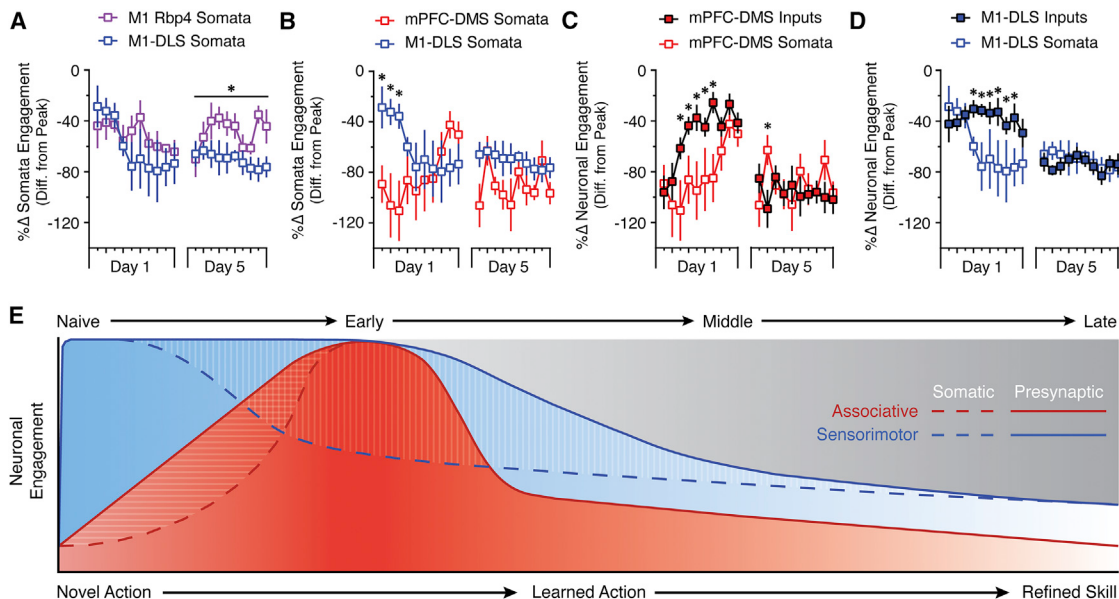


Figure 8. Neuronal Projection- and Compartment-Specific Activity Dynamics in Corticostriatal Projections Encode Action Learning

(A) Trial-related engagement (percent baseline $\Delta F/F$ during rotarod performance) in M1 Rbp4 somata and M1-DLS somata mice normalized to their peak individual trial-related engagement (group \times day interaction, $F_{1,207} = 4.110$, $p < 0.05$, HLMM; *different from M1-DLS somata, $p < 0.05$).

(B) Trial-related engagement in mPFC-DMS somata and M1-DLS somata mice normalized to their peak individual trial-related engagement (group \times day \times trial interaction, $F_{18,281} = 2.204$, $p < 0.005$, HLMM; *different from mPFC-DMS somata, $p < 0.05$).

(C) Trial-related engagement in mPFC-DMS inputs and mPFC-DMS somata mice normalized to their peak individual trial-related engagement (group \times day \times trial interaction, $F_{18,355} = 1.659$, $p < 0.05$, HLMM; *different from mPFC-DMS somata, $p < 0.05$).

(D) Trial-related engagement in M1-DLS inputs and M1-DLS somata mice normalized to their peak individual trial-related engagement (group \times day \times trial interaction, $F_{18,223} = 1.642$, $p < 0.05$, HLMM; *different from M1-DLS somata, $p < 0.05$). Data in (A)–(D) are presented as mean \pm SEM.

(E) Model of corticostriatal projection encoding of action learning showing parallel, but dissociable, activity dynamics within associative and sensorimotor somata and presynaptic elements as novel actions are refined into motor skills.

(DLS/putamen) in late stages of procedural learning (Miyachi et al., 2002; Yin et al., 2009; Lohse et al., 2014; Lehéricy et al., 2005; Floyer-Lea and Matthews, 2005) and therefore calls for refinement of a prominent conceptualization of the neural basis of skill learning.

Reconciling diminished sensorimotor cortical drive with such reports of heightened postsynaptic and regional striatal activity late in action learning likely implicates postsynaptic potentiation within the sensorimotor striatum (Yin et al., 2009; Dang et al., 2006; Wu et al., 2008, 2015). Indeed, reduced presynaptic sensorimotor input activity concurrent with postsynaptic potentiation is consistent with reports that M1 “tutors” subcortical circuits to more autonomously mediate the execution of learned motor sequences (Kawai et al., 2015). Moreover, such a combination of physiological processes aligns well with reports of reduced overall brain activity and enhanced sensorimotor network connectivity that develops across the learning of a refined motor skill (Coynel et al., 2010; Koralek et al., 2013; Bassett et al., 2015; Wu et al., 2004, 2008, 2015). Future studies probing the real-time activity of other striatal inputs (e.g., from somatosensory cortex, thalamus; for anatomical review, see McGeorge and Faull, 1989; Smith et al., 2004) may also reveal a contribution for other sources of excitatory drive over the sensorimotor striatum late in skill learning.

Although both mPFC-DMS and M1-DLS projections show pronounced disengagement across skill learning, mPFC-DMS

input disengagement selectively correlated with and predicted the rate and extent of this learning. Resonant with the notion that excessive and prolonged cognitive control of performance can impede efficient learning (Otto et al., 2015; Thompson-Schill et al., 2009), these findings suggest that activity of mPFC inputs to the DMS may help to gate the transition from unskilled to skilled performance. Relatedly, a recent human fMRI study showed that reductions in the integration of frontal and cingulate cortical networks during training of a motor skill predict individual differences in the rate of motor learning (Bassett et al., 2015).

The predictive relationship between mPFC-DMS input disengagement and skill learning provides important insight into the neural control of actions. Specifically, it suggests that the influence of associative inputs on action learning is transient, predominantly occurs early in learning, and modulates improvements in performance, likely via dynamic interaction with sensorimotor and other circuits. Indeed, the strong performance-related activity in M1-DLS inputs suggests that sensorimotor circuits also serve important roles during early learning (see also lesion studies from Yin et al., 2009). Thus, our findings do not provide direct support for the view that neural control of actions shifts from associative to sensorimotor circuits across learning (Miyachi et al., 2002; Graybiel, 2008; Yin et al., 2009) or that the two circuits necessarily compete for control of actions (Yin et al., 2009; Thorn et al., 2010; Thorn and Graybiel, 2014). In fact, no correlation was observed between M1-DLS input activity

dynamics and rotarod performance. Thus, no evidence of such a shift or competition is borne out by our data. Moreover, the predominantly parallel dynamics we report within these discrete circuits indicate that any shift of neural control or competition that does occur between associative and sensorimotor circuits does not manifest as opposing patterns of corticostratial input activity.

Corticostratial inputs are potently modulated at the level of their presynaptic terminals (Calabresi et al., 1990; Lovinger, 1991; Atwood et al., 2014; Park et al., 2014), and several of these modulatory processes have been implicated in action learning (Yin et al., 2009; Kheirbek et al., 2009; Hawes et al., 2015). Thus, we sought to probe for presynaptic modulation of corticostratial projections *in vivo* during action learning. To do so, we monitored task-related changes in GCaMP6s fluorescence across rotarod learning from four interrelated cellular targets: DMS-targeting somata in mPFC, DLS-targeting somata in M1, mPFC-derived inputs to DMS, and M1-derived inputs to DLS. We then compared the relative dynamics of their fluorescent signals across learning. Because (1) the somatic and presynaptic photometric signals are reliable proxies for neuronal activity (Figures 2 and 3; Chen et al., 2013; Kupferschmidt and Lovinger, 2015); (2) the presynaptic signals are causally linked to activity of their upstream somata (Figures 2C–2F and 3); (3) the somatic and presynaptic signals respond proportionally to changes in activity (Figures 3 and 6F; Figure S3); and (4) many forms of presynaptic plasticity or modulation at corticostratial inputs involve changes in presynaptic Ca^{2+} that could be detected by photometry (Kupferschmidt and Lovinger, 2015; Park et al., 2014; Huang et al., 2001), we reasoned that divergence of the somatic and presynaptic signals across training may reflect learning-related presynaptic plasticity or modulation that alters the coupling of somatic to presynaptic activity.

We found that over extended periods of training, somatic and presynaptic signals within mPFC-DMS and M1-DLS projections showed comparable reductions in engagement, suggesting that both projections show overall (i.e., cortical and striatal) disengagement across action learning. In addition, presynaptic mPFC-DMS inputs were faster to reach peak engagement during early learning than were mPFC-DMS somata, and presynaptic M1-DLS inputs were slower to disengage during early learning than M1-DLS somata. These findings reveal a divergence of task-related somatic and presynaptic activity in both associative and sensorimotor projections during early action learning that is consistent with the occurrence of learning-related *in vivo* potentiation of presynaptic Ca^{2+} -related corticostratial function. Although many mechanisms could mediate this effect, including learning-related changes in striatal microcircuits that impinge on presynaptic corticostratial function (Lovinger, 2010; Kupferschmidt and Lovinger, 2015; Girasole and Nelson, 2015; Logie et al., 2013; Blomeley et al., 2015), one particularly intriguing mechanism may involve training-induced presynaptic corticostratial NMDA receptor-mediated Ca^{2+} influx and plasticity. Indeed, corticostratial inputs exhibit forms of synaptic potentiation following learning-related patterns of activity (DeCoteau et al., 2007; Tort et al., 2008) that are mediated by enhanced presynaptic Ca^{2+} influx via NMDA receptors (Park et al., 2014) and comparable forms that are altered in *ex vivo* brain slices from rodents in early phases of procedural training (Hawes et al., 2015).

One notable consideration when interpreting our observed divergence of somatic and presynaptic activity across learning as evidence of presynaptic modulation is whether we are sampling from adequately comparable populations of corticostratial neurons in our somatic and presynaptic recordings. We believe this to be the case (within current technological limitations), since in both the somatic and presynaptic preparations, we are labeling and targeting neurons (with virus and fiber placement) on the basis of their discrete corticostratial connectivity. Future advances in sensitivity/resolution of fluorescence detection/imaging permitting within-animal simultaneous recording from striatal target-defined cortical somata and their precise striatal presynaptic inputs may enable more direct testing of this point. A second consideration is whether divergence of the somatic and presynaptic signals across action learning could reflect a change in the population of action-encoding neurons that is averaged differently by our bulk fluorescence measures in cortex and striatum. We believe this is unlikely since variations in the intensity of electrical stimulation of cortex (which varies the volume of activated cortex and therefore is analogous to an expansion/reduction of the population of task-activated neurons) causes proportional changes in the magnitude (and no change in other characteristics) of the fluorescent signals detected in cortex and striatum (Figure 6E; Figure S3D). Nonetheless, future experiments will be directed at exploring the mechanistic basis of this intriguing neuronal compartment-specific phenomenon.

In summary, by designing and employing novel fiber photometry approaches, we measured real-time *in vivo* activity dynamics of discrete corticostratial projections and provide direct evidence that parallel processing of associative and sensorimotor input activity encodes and predicts skill learning. This evidence challenges and refines existing views of corticostratial function (Miyachi et al., 2002; Yin et al., 2009; Lohse et al., 2014; Lehéricy et al., 2005; Thorn et al., 2010; Bassett et al., 2015; Wu et al., 2008; Gobel et al., 2011). Thus, we propose an updated model of action learning in which transient cortical drive of the associative striatum and progressive reduction of activity in sensorimotor inputs occurs concurrently with postsynaptic potentiation in the sensorimotor striatum to efficiently encode actions (Figure 8E). Lastly, our findings reveal previously inaccessible neuronal projection- and compartment-specific processes that underlie normal cortico-basal ganglia function and provide a foundation for studying discrete circuit dysfunction in disorders of action control.

STAR★METHODS

Detailed methods are provided in the online version of this paper and include the following:

- KEY RESOURCES TABLE
- CONTACT FOR REAGENT AND RESOURCE SHARING
- EXPERIMENTAL MODEL AND SUBJECT DETAILS
- METHODS DETAILS
 - Viruses and Stereotaxic Injections
 - Stereotaxic Fiber Implantation
 - *In Vivo* Fiber Photometry Apparatus

- *In Vivo* Fiber Photometry Analysis
- Accelerating Rotarod
- Video Analysis of Rotarod Behavior
- *In Vivo* Anesthetized Field and Photometry Recordings
- Estimating Detection Volume of Fiber Photometry System
- Immunohistochemistry and Histology
- Whole-Cell Brain Slice Electrophysiology
- Drugs

● QUANTIFICATION AND STATISTICAL ANALYSIS

SUPPLEMENTAL INFORMATION

Supplemental Information includes seven figures and can be found with this article online at <https://doi.org/10.1016/j.neuron.2017.09.040>.

AUTHOR CONTRIBUTIONS

D.A.K. and D.M.L. conceived the project. D.A.K., G.C., and D.M.L. designed and constructed the photometry system. K.J. and D.A.K. performed and analyzed the *in vivo* anesthetized field and photometry experiments. K.A.J. performed and analyzed the brain slice whole-cell electrophysiology experiments. D.A.K. performed and analyzed all other experiments. D.A.K. and D.M.L. wrote the manuscript with input from K.J., K.A.J., and G.C.

ACKNOWLEDGMENTS

We thank all members of the Lovinger laboratory for their generous and helpful discussions, feedback, and technical training, particularly Dr. Margaret Davis, Dr. Brian N. Mathur, and Dr. Matthew J. Pava. We also thank Guoxiang Luo for help with mouse genotyping and the Fishers Lane Animal Care staff for their exceptional animal husbandry. We thank the Genetically-Encoded Neuronal Indicator and Effector (GENIE) Project and the Janelia Farm Research Campus of the Howard Hughes Medical Institute for the GCaMP6 construct. We also thank Rachael Neve at the MIT McGovern Institute Viral Gene Transfer Core for the Cre-encoding HSV. This work was supported by the Division of Intramural Clinical and Biological Research of the NIAAA (ZIA AA000416) and the Natural Sciences and Engineering Research Council (NSERC) of Canada (PDF 438487-13).

Received: November 23, 2016

Revised: July 20, 2017

Accepted: September 22, 2017

Published: October 11, 2017

SUPPORTING CITATIONS

The following reference appears in the Supplemental Information: [Kupferschmidt et al. \(2015\)](#).

REFERENCES

- Atwood, B.K., Lovinger, D.M., and Mathur, B.N. (2014). Presynaptic long-term depression mediated by Gi/o-coupled receptors. *Trends Neurosci.* 37, 663–673.
- Bassett, D.S., Yang, M., Wymbs, N.F., and Grafton, S.T. (2015). Learning-induced autonomy of sensorimotor systems. *Nat. Neurosci.* 18, 744–751.
- Blomeley, C.P., Cains, S., and Bracci, E. (2015). Dual nitrergic/cholinergic control of short-term plasticity of corticostratial inputs to striatal projection neurons. *Front. Cell. Neurosci.* 9, 453.
- Calabresi, P., Mercuri, N.B., De Murtas, M., and Bernardi, G. (1990). Endogenous GABA mediates presynaptic inhibition of spontaneous and evoked excitatory synaptic potentials in the rat neostriatum. *Neurosci. Lett.* 118, 99–102.
- Cao, V.Y., Ye, Y., Mastwal, S., Ren, M., Coon, M., Liu, Q., Costa, R.M., and Wang, K.H. (2015). Motor learning consolidates arc-expressing neuronal ensembles in secondary motor cortex. *Neuron* 86, 1385–1392.
- Chen, T.W., Wardill, T.J., Sun, Y., Pulver, S.R., Renninger, S.L., Baohan, A., Schreiter, E.R., Kerr, R.A., Orger, M.B., Jayaraman, V., et al. (2013). Ultrasensitive fluorescent proteins for imaging neuronal activity. *Nature* 499, 295–300.
- Costa, R.M., Cohen, D., and Nicolelis, M.A. (2004). Differential corticostratial plasticity during fast and slow motor skill learning in mice. *Curr. Biol.* 14, 1124–1134.
- Coyne, D., Marrelec, G., Perlberg, V., Péligrini-Issac, M., Van de Moortele, P.F., Ugurbil, K., Doyon, J., Benali, H., and Lehéricy, S. (2010). Dynamics of motor-related functional integration during motor sequence learning. *Neuroimage* 49, 759–766.
- Cui, G., Jun, S.B., Jin, X., Pham, M.D., Vogel, S.S., Lovinger, D.M., and Costa, R.M. (2013). Concurrent activation of striatal direct and indirect pathways during action initiation. *Nature* 494, 238–242.
- Cui, G., Jun, S.B., Jin, X., Luo, G., Pham, M.D., Lovinger, D.M., Vogel, S.S., and Costa, R.M. (2014). Deep brain optical measurements of cell type-specific neural activity in behaving mice. *Nat. Protoc.* 9, 1213–1228.
- Dang, M.T., Yokoi, F., Yin, H.H., Lovinger, D.M., Wang, Y., and Li, Y. (2006). Disrupted motor learning and long-term synaptic plasticity in mice lacking NMDAR1 in the striatum. *Proc. Natl. Acad. Sci. USA* 103, 15254–15259.
- DeCoteau, W.E., Thorn, C., Gibson, D.J., Courtemanche, R., Mitra, P., Kubota, Y., and Graybiel, A.M. (2007). Oscillations of local field potentials in the rat dorsal striatum during spontaneous and instructed behaviors. *J. Neurophysiol.* 97, 3800–3805.
- Doyon, J., Bellec, P., Amsel, R., Penhune, V., Monchi, O., Carrier, J., Lehéricy, S., and Benali, H. (2009). Contributions of the basal ganglia and functionally related brain structures to motor learning. *Behav. Brain Res.* 199, 61–75.
- Foyer-Lea, A., and Matthews, P.M. (2005). Distinguishable brain activation networks for short- and long-term motor skill learning. *J. Neurophysiol.* 94, 512–518.
- Girasole, A.E., and Nelson, A.B. (2015). Probing striatal microcircuitry to understand the functional role of cholinergic interneurons. *Mov. Disord.* 30, 1306–1318.
- Gobel, E.W., Parrish, T.B., and Reber, P.J. (2011). Neural correlates of skill acquisition: decreased cortical activity during a serial interception sequence learning task. *Neuroimage* 58, 1150–1157.
- Graybiel, A.M. (2008). Habits, rituals, and the evaluative brain. *Annu. Rev. Neurosci.* 31, 359–387.
- Gremel, C.M., Chancey, J.H., Atwood, B.K., Luo, G., Neve, R., Ramakrishnan, C., Deisseroth, K., Lovinger, D.M., and Costa, R.M. (2016). Endocannabinoid modulation of orbitostriatal circuits gates habit formation. *Neuron* 90, 1312–1324.
- Gunaydin, L.A., Grosenick, L., Finkelstein, J.C., Kauvar, I.V., Fenno, L.E., Adhikari, A., Lammel, S., Mirzabekov, J.J., Airan, R.D., Zalocusky, K.A., et al. (2014). Natural neural projection dynamics underlying social behavior. *Cell* 157, 1535–1551.
- Haber, S.N., and Gdowski, M.J. (2003). The basal ganglia. In *The Human Nervous System, Second Edition*, G. Paxinos and J.K. Mai, eds. (Elsevier), pp. 676–738.
- Hawes, S.L., Evans, R.C., Unruh, B.A., Benkert, E.E., Gillani, F., Dumas, T.C., and Blackwell, K.T. (2015). Multimodal plasticity in dorsal striatum while learning a lateralized navigation task. *J. Neurosci.* 35, 10535–10549.
- Heindel, W.C., Butters, N., and Salmon, D.P. (1988). Impaired learning of a motor skill in patients with Huntington's disease. *Behav. Neurosci.* 102, 141–147.
- Hikosaka, O., Yamamoto, S., Yasuda, M., and Kim, H.F. (2013). Why skill matters. *Trends Cogn. Sci.* 17, 434–441.
- Huang, C.C., Lo, S.W., and Hsu, K.S. (2001). Presynaptic mechanisms underlying cannabinoid inhibition of excitatory synaptic transmission in rat striatal neurons. *J. Physiol.* 532, 731–748.

- Jueptner, M., Stephan, K.M., Frith, C.D., Brooks, D.J., Frackowiak, R.S., and Passingham, R.E. (1997a). Anatomy of motor learning. I. Frontal cortex and attention to action. *J. Neurophysiol.* 77, 1313–1324.
- Jueptner, M., Frith, C.D., Brooks, D.J., Frackowiak, R.S., and Passingham, R.E. (1997b). Anatomy of motor learning. II. Subcortical structures and learning by trial and error. *J. Neurophysiol.* 77, 1325–1337.
- Kawai, R., Markman, T., Poddar, R., Ko, R., Fantana, A.L., Dhawale, A.K., Kampff, A.R., and Ölveczky, B.P. (2015). Motor cortex is required for learning but not for executing a motor skill. *Neuron* 86, 800–812.
- Kelly, A.M., and Garavan, H. (2005). Human functional neuroimaging of brain changes associated with practice. *Cereb. Cortex* 15, 1089–1102.
- Kheirbek, M.A., Britt, J.P., Beeler, J.A., Ishikawa, Y., McGehee, D.S., and Zhuang, X. (2009). Adenylyl cyclase type 5 contributes to corticostratial plasticity and striatum-dependent learning. *J. Neurosci.* 29, 12115–12124.
- Koralek, A.C., Costa, R.M., and Carmena, J.M. (2013). Temporally precise cell-specific coherence develops in corticostratial networks during learning. *Neuron* 79, 865–872.
- Kupferschmidt, D.A., and Lovinger, D.M. (2015). Inhibition of presynaptic calcium transients in cortical inputs to the dorsolateral striatum by metabotropic GABA_B and mGlu2/3 receptors. *J. Physiol.* 593, 2295–2310.
- Kupferschmidt, D.A., Cody, P.A., Lovinger, D.M., and Davis, M.I. (2015). Brain BLAQ: post-hoc thick-section histochemistry for localizing optogenetic constructs in neurons and their distal terminals. *Front. Neuroanat.* 9, 6.
- Lehéricy, S., Benali, H., Van de Moortele, P.F., Pélérin-Issac, M., Waechter, T., Ugurbil, K., and Doyon, J. (2005). Distinct basal ganglia territories are engaged in early and advanced motor sequence learning. *Proc. Natl. Acad. Sci. USA* 102, 12566–12571.
- Logie, C., Bagetta, V., and Bracci, E. (2013). Presynaptic control of corticostratial synapses by endogenous GABA. *J. Neurosci.* 33, 15425–15431.
- Lohse, K.R., Wadden, K., Boyd, L.A., and Hodges, N.J. (2014). Motor skill acquisition across short and long time scales: a meta-analysis of neuroimaging data. *Neuropsychologia* 59, 130–141.
- Lovinger, D.M. (1991). Trans-1-aminocyclopentane-1,3-dicarboxylic acid (t-ACPD) decreases synaptic excitation in rat striatal slices through a presynaptic action. *Neurosci. Lett.* 129, 17–21.
- Lovinger, D.M. (2010). Neurotransmitter roles in synaptic modulation, plasticity and learning in the dorsal striatum. *Neuropharmacology* 58, 951–961.
- Masamizu, Y., Tanaka, Y.R., Tanaka, Y.H., Hira, R., Ohkubo, F., Kitamura, K., Isomura, Y., Okada, T., and Matsuzaki, M. (2014). Two distinct layer-specific dynamics of cortical ensembles during learning of a motor task. *Nat. Neurosci.* 17, 987–994.
- Mazzoni, P. (2008). Efficient motor control: how can less be more? *J. Physiol.* 586, 4031.
- McGeorge, A.J., and Faull, R.L. (1989). The organization of the projection from the cerebral cortex to the striatum in the rat. *Neuroscience* 29, 503–537.
- Miyachi, S., Hikosaka, O., Miyashita, K., Kárádi, Z., and Rand, M.K. (1997). Differential roles of monkey striatum in learning of sequential hand movement. *Exp. Brain Res.* 115, 1–5.
- Miyachi, S., Hikosaka, O., and Lu, X. (2002). Differential activation of monkey striatal neurons in the early and late stages of procedural learning. *Exp. Brain Res.* 146, 122–126.
- Otto, A.R., Skatova, A., Madlon-Kay, S., and Daw, N.D. (2015). Cognitive control predicts use of model-based reinforcement learning. *J. Cogn. Neurosci.* 27, 319–333.
- Park, H., Popescu, A., and Poo, M.M. (2014). Essential role of presynaptic NMDA receptors in activity-dependent BDNF secretion and corticostratial LTP. *Neuron* 84, 1009–1022.
- Pearson, K. (1901). On lines and planes of closest fit to systems of points in space. *The London, Edinburgh, and Dublin Philosophical Magazine and Journal of Science* 2, 559–572.
- Poldrack, R.A., Sabb, F.W., Foerde, K., Tom, S.M., Asarnow, R.F., Bookheimer, S.Y., and Knowlton, B.J. (2005). The neural correlates of motor skill automaticity. *J. Neurosci.* 25, 5356–5364.
- Smith, Y., Raju, D.V., Pare, J.F., and Sidibe, M. (2004). The thalamostriatal system: a highly specific network of the basal ganglia circuitry. *Trends Neurosci.* 27, 520–527.
- Stefanova, E.D., Kostic, V.S., Ziropadja, L., Markovic, M., and Ocic, G.G. (2000). Visuomotor skill learning on serial reaction time task in patients with early Parkinson's disease. *Mov. Disord.* 15, 1095–1103.
- Thompson-Schill, S.L., Ramscar, M., and Chrysikou, E.G. (2009). Cognition without control: when a little frontal lobe goes a long way. *Curr. Dir. Psychol. Sci.* 18, 259–263.
- Thorn, C.A., and Graybiel, A.M. (2014). Differential entrainment and learning-related dynamics of spike and local field potential activity in the sensorimotor and associative striatum. *J. Neurosci.* 34, 2845–2859.
- Thorn, C.A., Atallah, H., Howe, M., and Graybiel, A.M. (2010). Differential dynamics of activity changes in dorsolateral and dorsomedial striatal loops during learning. *Neuron* 66, 781–795.
- Tort, A.B., Kramer, M.A., Thorn, C., Gibson, D.J., Kubota, Y., Graybiel, A.M., and Kopell, N.J. (2008). Dynamic cross-frequency couplings of local field potential oscillations in rat striatum and hippocampus during performance of a T-maze task. *Proc. Natl. Acad. Sci. USA* 105, 20517–20522.
- Wilson, C.J. (1995). The contribution of cortical neurons to the firing pattern of striatal spiny neurons. In *Models of Information Processing in the Basal Ganglia*, J.C. Houk, J.L. Davis, and D.G. Beiser, eds. (MIT Press), pp. 29–50.
- Wu, T., Kansaku, K., and Hallett, M. (2004). How self-initiated memorized movements become automatic: a functional MRI study. *J. Neurophysiol.* 91, 1690–1698.
- Wu, T., Chan, P., and Hallett, M. (2008). Modifications of the interactions in the motor networks when a movement becomes automatic. *J. Physiol.* 586, 4295–4304.
- Wu, T., Hallett, M., and Chan, P. (2015). Motor automaticity in Parkinson's disease. *Neurobiol. Dis.* 82, 226–234.
- Yin, H.H., Mulcare, S.P., Hilário, M.R., Clouse, E., Holloway, T., Davis, M.I., Hansson, A.C., Lovinger, D.M., and Costa, R.M. (2009). Dynamic reorganization of striatal circuits during the acquisition and consolidation of a skill. *Nat. Neurosci.* 12, 333–341.

STAR★METHODS**KEY RESOURCES TABLE**

REAGENT or RESOURCE	SOURCE	IDENTIFIER
Antibodies		
Chicken polyclonal anti-GFP	Abcam	Ab13970; RRID: AB_300798
Rabbit polyclonal anti-Caspase-3 (active/cleaved form)	Millipore	AB3623; RRID: AB_91556
Alexa 488-conjugated goat anti-chicken	Thermo Fisher Scientific	A-11039; RRID: AB_2534096
Alexa 568-conjugated goat anti-rabbit	Thermo Fisher Scientific	A-11036; RRID: AB_10563566
Alexa 568-conjugated Isolectin GS-IB4	Molecular Probes	I21412
Bacterial and Virus Strains		
AAV1.CAG::FLEX.GCaMP6s	Penn Vector Core	AV-1-PV2818
AAV2/9.CAG::FLEX.eGFP	Penn Vector Core	N/A
HSV.hEF1 α ::IRES.Cre.mCherry	MIT McGovern Institute for Brain Research	N/A
Chemicals, Peptides, and Recombinant Proteins		
Picrotoxin	Sigma-Aldrich	P1675
Lidocaine Hydrochloride Monohydrate	Sigma-Aldrich	L5647
Urethane	Sigma-Aldrich	U2500
Experimental Models: Organisms/Strains		
Mouse: B6.129S2-Emx1tm1(cre)Krl/J	The Jackson Laboratory	JAX: 005628; RRID: IMSR_JAX:005628
Mouse: C57BL/6J	The Jackson Laboratory	000664; RRID: IMSR_JAX:000664
Mouse: B6.FVB(Cg)-Tg(Rbp4-cre)KL100Gsat/Mmucd	Charles Gerfen, GENSAT	N/A

CONTACT FOR REAGENT AND RESOURCE SHARING

Requests for further information should be directed to and will be fulfilled by the Lead Contact, David M. Lovinger (lovindav@mail.nih.gov).

EXPERIMENTAL MODEL AND SUBJECT DETAILS

Emx1::Cre (B6.129S2-Emx1tm1(cre)Krl/J) and C57BL/6J mice were purchased from the Jackson Laboratory (Bar Harbor, ME, USA). Rbp4::Cre mice (B6.FVB(Cg)-Tg(Rbp4-cre)KL100Gsat/Mmucd) were provided by Charles Gerfen at GENSAT. All Cre lines were backcrossed onto a C57BL/6J background for > 6 generations. Male and female Emx1::Cre, male Rbp4::Cre mice, and male C57BL/6J mice were housed 2-4/cage on a 12-h (06:30-18:30) light cycle with *ad libitum* access to rodent chow and water. Attempts were made to balance experimental groups by age, sex (Emx1::Cre mice), and housing condition. All behavioral studies were performed during the light phase. All animal protocols were approved by the US National Institute on Alcohol Abuse and Alcoholism (NIAAA) Animal Care and Use Committee and conducted in accordance with the National Institutes of Health (NIH) guidelines for animal research.

METHODS DETAILS**Viruses and Stereotaxic Injections**

Adeno-associated viruses (AAVs) encoding Cre-dependent GCaMP6s (AAV1.CAG::FLEX.GCaMP6s) and eGFP (AAV2/9.CAG::FLEX.eGFP) were purchased from Penn Vector Core (Philadelphia, PA, USA). Herpes-simplex virus encoding Cre (HSV-Cre; HSV.hEF1 α ::IRES.Cre.mCherry) was purchased from Rachael Neve at the MIT McGovern Institute for Brain Research. All viral constructs were injected at titers > 10¹² genome copies/mL. All stereotaxic viral injections were conducted using aseptic surgical technique. Mice (age 6-14 weeks) were deeply anesthetized with 5% isoflurane in oxygen (v/v) and secured in a stereotaxic frame (Kopf Instruments, Germany). Sedation was maintained at 1%-2% isoflurane during surgery. A midline incision was made on the scalp and bilateral craniotomies were performed above the target regions. Bilateral injection coordinates for each region were (A/P, M/L from

Bregma, D/V from brain surface, in mm): mPFC ($+1.5, \pm 0.3, -2.1$); M1 ($+1.0, \pm 1.5, -1.0$); DMS ($+1.0, \pm 1.2, -2.3$); DLS ($+0.6, \pm 2.4, -2.5$). Viruses were microinjected using a 25-gauge syringe (86250, Hamilton) at a rate of 50 nL/min. GCaMP6s virus was injected bilaterally into mPFC or M1 at volumes of 200 or 300 nL/site, respectively. HSV-Cre was injected bilaterally into either DMS or DLS at a volume of 400 nL/site. After infusion, the needle was left in place for 5 min to allow for virus diffusion before the needle was slowly withdrawn. Incisions were closed and secured with VetBond tissue adhesive (1469Sb, 3M). Mice injected with GCaMP6s alone recovered for 6–8 weeks prior to fiber implantation; mice injected with HSV-Cre and GCaMP6s recovered for 8–10 weeks prior to implantation.

Stereotaxic Fiber Implantation

Using aseptic surgical technique and under isoflurane anesthesia, the skulls of previously injected mice were re-exposed and fitted with two miniature screws (Antrin Miniature Specialties, Inc.). Mice were implanted with an optical fiber (FG105UCA, ThorLabs) secured within a 2.5-mm ceramic ferrule (CF128, 2.5 mm OD, 128 μm ID, ThorLabs) using fiber epoxy (F112, ThorLabs). Implant coordinates were approximately (A/P, M/L from Bregma, D/V from brain surface, in mm): mPFC ($+1.5, \pm 0.3, -0.8$); M1 ($+1.0, \pm 1.5, -0.5$); DMS ($+1.0, \pm 1.2, -1.8$); DLS ($+0.6, \pm 2.4, -2.0$). For simultaneous M1 microinfusions and DLS photometry, cannulas (C315GS-5-SP, Plastics One) were implanted at a 15° angle in M1 ($+1.0, \pm 1.0, -0.8$), and fibers at an opposing 15° angle into DLS ($+0.6, \pm 2.8, -1.8$). Fluorescence was detected by the fiber photometry system during implantation to guide optimal fiber placement. Dental cement was used to adhere the ferrule/fiber to the skull. Following surgery, mice were returned to group housing and left to recover for at least 1 week prior to behavioral testing and photometric recording. Approximately 20% of mice injected with GCaMP and implanted with an optical fiber exhibited GCaMP6s fluorescence that was detectable (generated a fluorescence spectrum that differed from background autofluorescence) and activity dependent (i.e., depressed by isoflurane or increased during rapid movements, and engaged above baseline during any of the 10 trials on day 1 of rotarod training). Insufficient GCaMP6s expression or misplaced fiber implantation, as confirmed by histological assessment of several unused mice, accounted for this success rate.

In Vivo Fiber Photometry Apparatus

Blue light from a 473-nm picosecond-pulsed laser (20 MHz; BDL-473-MC, Becker & Hickl) was directed into a cage cube (CM1-DCH, ThorLabs) onto a GFP dichroic filter (MD498, ThorLabs), and coupled using a FC/PC fiber coupler (PAFA-X-4-A, ThorLabs) into a multimode fiber patch cord (FG105UCA, 0.22 NA, 105/125 μm diameter core/cladding, ThorLabs) terminating in a ceramic ferrule (Cui et al., 2014; CF128, ThorLabs). On each recording day, the ferrule end of the patch cord and the surgically implanted ferrule were cleaned with lens cleaner and paper (80919 and 806, Ted Pella), lightly coated with an index matching oil (Immersol 518F, Zeiss), and securely attached via a mating sleeve (ADAF1, ThorLabs). The continuous-wave-equivalent power of the light used to excite GCaMP6s in the brain was approximately 0.1 mW at the free end of the fiber. Fluorescence emission from the tissue was collected by the same fiber, directed using a fiber coupler (PAF-SMA-11-A, Thorlabs) into a 200- μm diameter core, anti-reflection-coated multimode fiber (M200L02S-A, ThorLabs), filtered through a 485-nm long-pass filter, and dispersed into spectra by a polychromator (PML-SPEC, Becker & Hickl). Spectra were projected onto a 16-channel photomultiplier tube (PMT) array. The array spanned an adjustable 106-nm wavelength window that was centered around 525 nm (PML-16C, Becker & Hickl). Individual photons were detected in each PMT channel and recorded by a time-correlated single photon counting (TCSPC) module (SPC-830, Becker & Hickl) at a frequency of 20 Hz.

In Vivo Fiber Photometry Analysis

The shape, location, and amplitude of the TCSPC-derived fluorescence spectrum were used to confirm *in vivo* GCaMP6s expression. Custom data processing was used to calculate the integrated photon count of the fluorescence decay curves from select spectral channels as a measure of fluorescence intensity. Two spectral channels comprising the peak of the GCaMP6s spectrum served as ‘peak’ channels (~ 515 – 525 nm); these showed the strongest activity-dependent changes in fluorescence. Two shorter wavelength channels (~ 490 – 500 nm) that showed no activity-dependent changes in fluorescence intensity were labeled ‘off peak’ channels and served as a control signal for any movement artifacts. For rotarod trials, $\% \Delta F/F$ was calculated as the difference between the integrated photon count (F) and the median integrated photon count of a 40 s baseline period (F_{MBL}) prior to mouse placement on the accelerating rotarod, divided by this median: $\% \Delta F/F = [(F - F_{MBL})/F_{MBL}] * 100$. For *in vivo* anesthetized photometric recordings, F_{MBL} was calculated using F values from the 5-s period immediately preceding electrical stimulation.

Two main forms of activity-dependent changes in fluorescence were observed in our experimental mice during rotarod trials: sustained changes in steady state/basal fluorescence, and transient changes in fluorescence (called “events”). Sustained changes in fluorescence were commonly observed in groups targeted for presynaptic or somatic recordings; indeed, sustained increases in fluorescence often contained superimposed discrete fluorescent “events.” Changes in basal fluorescence predominated in mice targeted for associative and sensorimotor presynaptic inputs (mPFC-DMS and M1-DLS Inputs), whereas sustained and transient changes in fluorescence were routinely observed in mice targeted for associative and sensorimotor somata (mPFC-DMS and M1-DLS Somata). Thus, for consistency, and to directly compare presynaptic and somatic recordings, we calculated the average % baseline (BL) $\Delta F/F$ during rotarod performance (termed, task-related “engagement”) for all experimental preparations, and fluorescent event frequency and magnitude in somatic preparations as a supplemental measure of neuronal activity.

% BL ΔF/F was calculated for each rotarod trial using the fluorescent signal within the window from 10 s after trial onset to 10 s prior to trial termination. This window was selected to prevent contamination of the task-related signal by residual increases in GCaMP6 fluorescence induced by placement of the mouse on the rod, or any aberrant signal changes induced by variable and complex dismounts from the rod at the end of the trial. To calculate the slope of the presynaptic fluorescence, linear regressions were conducted for each rotarod trial using %ΔF/F values that spanned the window from 10 s after trial onset to 10 s prior to trial termination. To directly compare training-related fluorescence changes in two different neuronal preparations (e.g., %BL ΔF/F in mPFC-DMS Inputs versus M1-DLS Inputs), average trial %BL ΔF/F values of individual mice were normalized to the average trial %BL ΔF/F of their peak trial, and expressed as % change from peak trial, using the following equation: [(Trial %BL ΔF/F) - (Max Trial %BL ΔF/F)] / (Max Trial %BL ΔF/F) × 100.

To assess the frequency and magnitude of transient fluorescent events, %ΔF/F values were first baseline adjusted such that the minimum value in each trial was 0 (i.e., not negative). Acute fluctuations in %ΔF/F were considered fluorescent events if: [1] the interrogated %ΔF/F value was greater than $\mu_{BL} + 3\sigma_{BL}$, where μ_{BL} and σ_{BL} were the mean and standard deviation of the 400-ms period of %ΔF/F values preceding the interrogated value; [2] the maximum of the 500-ms period of %ΔF/F values following the interrogated %ΔF/F value was greater than $\mu_{BL} + 5\sigma_{BLTOT}$, where σ_{BLTOT} is the average standard deviation of all 400-ms periods preceding the putative fluorescent events as determined by criteria #1; [3] no fluorescent events were assigned within the 400-ms period preceding the interrogated %ΔF/F value. ‘Baseline events’ were those occurring within the 40 s baseline period prior to mouse placement on the accelerating rotarod. ‘Trial events’ were those occurring within the window from 10 s after trial onset to 10 s prior to trial termination. A ‘rate modulation index’ was calculated as [(Trial Event Rate) - (Baseline Event Rate)] / [(Trial Event Rate) + (Baseline Event Rate)] × 100.

To correlate photometric data with behavior, input disengagement rates were calculated for each mouse as [1 - (# of Trials from Peak %BL ΔF/F to Minimum %BL ΔF/F)/49], where 49 represents the maximum possible number of trials following the trial with Peak %BL ΔF/F. Learning rates from the same point in training (Trial with Peak %BL ΔF/F) were calculated as [1 - (# of Trials from Peak %BL ΔF/F to Peak Latency to Fall)/49].

Accelerating Rotarod

Mice were connected to an optical fiber and habituated for two daily 2-h periods at the base of a customized, computer-interfaced rotarod (EZRod, Omnitech Electronics) prior to day 1 of rotarod training. Every training day began with 1 h of habituation at the rotarod base. The blue laser was turned on for the final 30 min of this period to ensure stable photometric recordings that were uninfluenced by GCaMP6s fluorescence bleaching (Figure S4H). A TTL pulse from the rotarod triggered the TCSPC system to record fluorescence in 7-min blocks comprised of: a 40 s baseline period during which mice were at the rotarod base, a 20 s period during which mice were placed on rotating rod (4 rpm), a trial period of up to 300 s over which the rotarod accelerated from 4–40 rpm, and a post-trial period of at least 60 s. Mice were trained for 10 trials/day for 5 days using this 4–40 rpm paradigm. Trials were conducted every 10 min. Latency to fall from the rotarod was recorded during each trial. Individual trials were stopped and latency was recorded if mice held onto the rod for two consecutive rotations or reached 40 rpm. Mice were randomly assigned to undergo photometric recordings either on each of the 5 training days (D1–5), or on days 1 and 5 only (D1+5; Figure 4H; Figures S4E, S7G, and S7H). Given no effect of additional laser exposure time (D2–4) on training-related changes in GCaMP6s fluorescence in the mPFC-DMS and M1-DLS input groups (Figure 4H), data from mice in each of the mPFC-DMS and M1-DLS somata groups that underwent photometric recordings on D1–5 ($n = 3$ per group; Figures S7G and S7H) were combined with those that underwent photometric recordings on D1+5 ($n = 7$ and 4 per group; Figure 7). Following training on the 4–40 rpm paradigm, a random subset of mice was subsequently trained on a double acceleration 8–80 rpm paradigm and a constant 25 rpm paradigm.

Video Analysis of Rotarod Behavior

A high-definition camera (Med Associates) was mounted in view of the rotarod apparatus. Videos of a cohort of mice ($n = 4$) performing on the rotarod were recorded during all trials. As described by Cao et al. (2015), foot position was measured using video-tracking software, Tracker (Douglas Brown, Open Source Physics). The first 60 s of each trial was analyzed (60 s corresponded to a period during which all mice stayed on the rotarod). The distance from the left rear paw to the top of the 3-cm rod was measured every two seconds. The average foot position and standard deviation of foot position during this 60-s time period was calculated.

In Vivo Anesthetized Field and Photometry Recordings

Emx1::Cre, Rbp4::Cre, and C5BL/6J mice injected at age 6–14 weeks with GCaMP6s virus (see above for brain targets) underwent *in vivo* electrophysiology and photometry recordings at age 23–37 weeks (>6 weeks post-injection). Mice were pre-anesthetized with 5% isoflurane (v/v) in oxygen, injected with urethane (1.5 g/kg, i.p.), and secured in a stereotaxic frame. Isoflurane was supplied during craniotomy procedures at 0.5%–2.0% (v/v) followed by oxygen upon completion. Isoflurane was provided to deepen the initial anesthesia level and ensure that mice felt no pain during the surgery. Oxygen was provided to improve the general condition of the mouse during recordings. Depth of anesthesia was monitored by regular hind leg withdrawal reflex tests and breathing rate assessments. A supplementary urethane injection (10% of initial dose) was administered if anesthesia depth diminished. Mouse body temperature was maintained at 37°C using a heating pad and DC Temperature Control System (FHC, USA). Craniotomies were performed using a dental drill (Osada, Japan) above target regions (A/P, M/L from Bregma, D/V from brain surface, in mm):

stimulating electrode (25° angle) in mPFC (+1.5 to +1.7, +0.9 to 1.0, -1.9 to -2.2) or M1 (+1.0, +1.8 to 2.0, -0.9); recording electrode (10° angle) in DMS (+0.9 to 1.0, +1.8, -1.8 to -2.2) or DLS (+0.0, +3.0, -1.8 to -2.4); optical fiber (0° angle) in DMS (+0.8 to 1.2, +1.2, -1.9 to -2.5) or DLS (+0.6 to +1.0, +2.4, -1.9 to -2.5). Electrophysiological recordings of electrically-evoked field potentials (eFPs) were collected using a glass pipette (resistance ~2 MΩ) pulled from borosilicate filamented glass (WPI, USA) on a Sutter P-97 puller (Sutter Instruments, USA) and filled with 0.9% sodium chloride (Hospira, USA). Electrically-evoked photometric responses were recorded using an optical fiber (FG105UCA, 0.22 NA, 105/125 μm diameter core/cladding, ThorLabs) connected to the TCSPC fiber photometry system used for freely moving recordings. Electrical stimulation was generated by a stimulus isolator (Isoflex, A. M. P. I., Israel) controlled by pClamp 9.2 software (Molecular Devices, USA) and delivered to the brain by a twisted bipolar tungsten electrode (PlasticsOne, USA) placed in cortex. Following recording, the optical fiber and recording glass capillary were removed from the brain, immersed in red fluorescent 1,1'-dioctadecyl-3,3',3'-tetramethylindocarbocyanine perchlorate (Di-I, Molecular probes, USA) dissolved in acetone (100 mg/mL), air-dried for 2-3 min, and placed again in the brain at the same depth (for 2-3 repetitions) to allow post-mortem verification of recording sites. Mice were euthanized with an overdose of urethane and transcardially perfused with 0.1 M PBS and 4% formaldehyde. Brains were collected and post-fixed in 4% formaldehyde at 4°C for 24 h prior to brain slicing and histological assessment. Stimulating electrode placement was verified by visual examination of tissue damage. Electrophysiological signal was acquired using an Axoclamp 2A amplifier, Digidata 1332a digitizer, and pClamp 9.2 software (Molecular Devices, USA).

Estimating Detection Volume of Fiber Photometry System

Mice expressing GFP in dopamine D2-receptor expressing neurons in the striatum (D2::GFP mice) were sacrificed, and their brains were excised, blocked near the bottom quarter of the striatum, and thinly glued to an opaque plastic dish (Figure S2). D2::GFP mice were used to estimate the volume of brain tissue from which the fiber photometry system detects fluorescence because they express GFP relatively homogenously throughout the striatum. To estimate the maximum detection depth of the fiber photometry system (Cui et al., 2013), an optical fiber was lowered through the fluorescent striatum toward the opaque surface. Prior to the depth at which the base of the cone of fluorescence detection reaches the opaque surface, the photon count should remain constant. Beyond this depth, the photon count should reduce as the number of fluorophores residing within the detection cone becomes progressively smaller. The detection depth was therefore estimated as the distance between the depth at which the photon count starts to decrease and the depth at which it nears zero. To estimate the width of the cone of fluorescence detection, D2::GFP mouse brains were mounted on a vibratome, an optical fiber was implanted horizontally into the middle of the striatum, and 50-μm horizontal slices were removed from the brain surface toward the fiber. Prior to the depth at which the widest portion of the detection cone is reached by the vibratome, the photon count should remain constant. Beyond this depth, the photon count should lessen as the number of fluorophores residing within the detection cone diminishes. The width of the detection cone was therefore estimated as the distance between the depth at which the photon count starts to decrease and the depth at which it is reduced by 50% (or when the vibratome blade hit the optical fiber). To assess any contribution of striatal fluorescence to the photometry signal detected from within cerebral cortex, photometric measurements were made as an optical fiber was lowered from the surface of D2::GFP brains into the striatum.

Immunohistochemistry and Histology

For histology of viral expression and fiber placement, and immunohistochemical characterization of potential GCaMP6s-associated neuronal toxicity, mice were transcardially perfused under deep sodium pentobarbital anesthesia with room temperature 0.1 M PBS and 4% formaldehyde in PBS (pH 7.4). Brains were collected and post-fixed in 4% formaldehyde at 4°C for 24 h. 50- to 100-μm coronal sections were made using a vibratome through frontal cortex and striatum. On a revolving platform, sections were incubated for 4 h in PBST (PBS with 0.2% Triton X-100), and blocked in 5% bovine serum albumin in PBST for 8 h. Sections were then incubated in chicken polyclonal anti-GFP (1:2000, ab13970, Abcam) and/or rabbit polyclonal anti-Caspase 3 (active/cleaved form, 1:100, AB3623, Millipore) in PBST for 12-16 h at 4°C. Following three 1-h washes in PBST, sections were incubated in Alexa Fluor 488-conjugated goat anti-chicken antibody (1:2000, A-11039, ThermoFisher Scientific), Alexa 568-conjugated goat anti-rabbit antibody (1:2500, A-11036, ThermoFisher Scientific), and/or Alexa Fluor 568-conjugated Isolectin GS-IB4 (1:1000, I21412, Molecular Probes) in PBST for 16 h at 4°C. Following a 1-h wash in PBST containing 4',6-diamidino-2-phenylindole (DAPI; 1:20,000 of 5 mg/mL, D3571, Molecular Probes) and two 1-h washes in PBS, sections were mounted on Superfrost Plus slides (EF15978Z, Daigger) using Fluoromount Aqueous Mounting Medium (F4680, Sigma), coverslipped, and imaged using Zeiss AxioVision LE 4.3 software with a Zeiss AxioCam on a Zeiss SteREO Lumar microscope (for Figure S1 histology), or ZEN 2012 software with a confocal LSM880 microscope (for Figure S5 toxicity analysis). Background was subtracted for presentation.

Whole-Cell Brain Slice Electrophysiology

Coronal brain slices (220 μm thick) were prepared from 8-month old Rbp4::Cre mice (n = 3) injected with AAV1.CAG::FLEX.GCaMP6s virus into bilateral M1 using a vibratome (Leica Microsystems) as previously described. Following isoflurane anesthesia, mice were decapitated and brains were rapidly removed and submerged in ice-cold cutting solution containing (in mM): 30 NaCl, 4.5 KCl, 1 MgCl₂, 26 NaHCO₃, 1.2 NaH₂PO₄, 10 glucose, and 194 sucrose, continuously bubbled with 95% O₂/5% CO₂. Slices were removed to a 32°C holding chamber containing artificial cerebrospinal fluid (aCSF) containing (in mM): 124 NaCl, 2.5 KCl, 2 CaCl₂, 1 MgCl₂, 26

NaHCO₃, 1.2 NaH₂PO₄, and 12.5 glucose, continuously bubbled with 95% O₂/5% CO₂. Slices were incubated for 30 minutes at 32°C, and then were held at room temperature for 1–5 hours prior to experiments.

Individual hemisected slices were placed in a diamond-shaped recording chamber (Warner Instruments) and were submerged in, and continuously perfused with 30–32°C aCSF at a rate of ~1.5 mL/min. Recording pipettes (3.0–4.0 MΩ resistance in bath) were filled with internal solution (295–300 mOsm) containing (in mM): 120 K-gluconate, 4 NaCl, 20 KCl, 10 HEPES, 0.4 Na-GTP, and 4 Mg-ATP; pH was adjusted to 7.25 using KOH. Slices were visualized on a Zeiss Axioskop 2 microscope. GCaMP6s-positive or negative layer V pyramidal cells in M1 were visualized using a 40x/0.8 NA water-immersion objective. Expression of GCaMP6s was determined by the observation of fluorescence in recorded neurons, as well as a qualitative assessment of increased fluorescence intensity upon depolarizing current injections in current-clamp mode that elicited firing at 10–20 Hz. Acquisition was performed using Clampex 10.3 (Molecular Devices). Resting membrane potentials were recorded 5 min after break-in. Intrinsic properties were studied by injecting a series of currents starting at –200 pA and increasing in 50-pA steps up to 400 pA with a duration of 1 s. Action potentials elicited by each current injection were averaged for two trials per cell. Input resistance was determined by plotting the current-voltage relationship for hyperpolarizing and subthreshold depolarizing steps during the late (steady-state) component of the response and obtaining the slope of a least-squares linear fit of the data points for each cell. Data were analyzed using Clampfit 10.3.

Drugs

Picrotoxin (P1675, Sigma) was dissolved in saline at a concentration of 0.25 μg/μL, and injected (i.c.) into M1 at a volume of 0.3 μL. Lidocaine hydrochloride monohydrate (L5647, Sigma) was dissolved to a 5% solution in saline, and injected (i.c.) into M1 at a volume of 0.3 μL. Urethane (U2500, Sigma) was dissolved in dH₂O at a concentration of 0.25 g/mL, and injected at a volume of 6 mL/kg (i.p.).

QUANTIFICATION AND STATISTICAL ANALYSIS

Data are presented as means ± SEM. One-sample Student's t tests were used for comparisons of a single group to a set value. Two-tailed paired or unpaired Student's t tests were used for comparisons of only two groups. Repeated-measures comparisons across individual trials (e.g., comparisons of rotarod latency in mPFC-DMS mice; comparisons of %baseline fluorescence in mPFC-DMS versus M1-DLS inputs) were conducted using a hierarchical linear mixed model (HLM). For comparisons involving one experimental group, a model with two repeated, fixed factors was implemented to test for effects of Trial nested within Day. For comparisons involving two experimental groups, a model was implemented to examine the between-group interaction of Neuronal Population (e.g., mPFC-DMS inputs versus M1-DLS inputs) with repeated-measures of Trial nested within Day. All pairwise comparisons of the model-derived estimated marginal means underwent Bonferroni corrections, and all reported P values reflect these corrections. Pearson's correlations and Deming regressions (Pearson, 1901) were conducted to assess the relationship between two independent variables (e.g., learning versus disengagement rates). Statistical outliers were determined by Grubb's test (criterion of $\alpha = 0.05$). Effects were considered statistically significant at $p < 0.05$. Data were analyzed using Microsoft Excel, Python, GraphPad Prism 6 and PASW Statistics 18.